Anal. Methods Environ. Chem. J. 8 (3) (2025) 5-30

AMECJ

Research Article, Issue 3
Analytical Methods in Environmental Chemistry Journal
Journal home page: www.amecj.com/ir

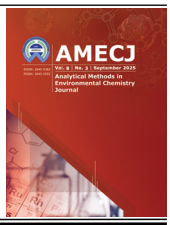

Determination and removal of cadmium and lead ions from aqueous solutions using surface-modified chitosan magnetic nanoparticles and flame atomic absorption spectroscopy

Nada Qasim Jebur [a], Ali Abdulrazzaq Abdulwahid [a,], and Hanna S. Abbo [a]**
[a] *University of Basrah, College of Science, Chemistry Department - Basrah, Iraq*

ARTICLE INFO:
Received 10 May 2025
Revised form 13 Jul 2025
Accepted 11 Aug 2025
Available online 30 Sep 2025

Keywords:
Nanomagnetic chitosan,
Flame Atomic absorption spectroscopy,
Isotherm models,
Adsorption thermodynamics

ABSTRACT
Nanomagnetic chitosan composites (NMCC) adsorbents were synthesized by the hydrothermal method with chitosan, ethylene diamine tetraacetic acid, and 3,3´-diaminobenzidine, and the adsorption efficiencies for the removal of cadmium and lead ions from aqueous solution were investigated. The prepared adsorbents were characterized using FTIR, high-resolution transmission electron microscopy (HRTEM), and energy-dispersive X-ray (EDX). Batch systems were carried out, and different operation parameters, including pH, agitation time, and temperature, were optimized. It was observed that the maximum removal efficiency was obtained at pH 8.0 and 5.0, and with agitation time (6, 3, 1) hr. and (2, 1.5, 1) hr. for Cd2+ and Pb2+, respectively. Langmuir, Freundlich, Dubinin-Radushkevich, and Temkin isotherm models were applied, and the results showed that Langmuir was fitted very well for all adsorption systems. From the linearized Langmuir equation, q_{max} was 54.64, 81.97, and 344.8 mg g^{-1} for cadmium ion and 222.2, 344.8, and 714.3 mg g^{-1} for lead onto Ch@F, Ch@EDTA@F, and Ch@EDTA@Am.@F, respectively. Kinetic models were employed to elucidate the adsorption mechanisms. The pseudo-second-order model demonstrated a good agreement with experimental data for both Cadmium and Lead ions across all adsorbents. Adsorption systems results were further evaluated by calculating thermodynamic parameters, including enthalpy, entropy, changes in free energy, and activation energy, Ea.

1. Introduction

Since the late 18th century, when the Industrial Revolution started, pollution has grown to be one of the world's most significant problems. This is because agriculture, urbanization, and industrialization are all developing quickly on a global scale. The scientific community has been interested in cadmium and lead poisoning because of the possible harm they could do to human health and the environment. This kind of pollution has the potential to spread throughout the biosphere, atmosphere, lithosphere, and hydrosphere, among other components of the Earth's system [1]. Low levels of exposure to these metals have been linked to a number of illnesses and even death, according to newly established tools and procedures for measuring these compounds. However, the literature has extensively documented that lead and cadmium pollute several environmental

*Corresponding Author: Ali Abdulrazzaq Abdulwahid
Email: ali.abdulwahid@uobasrah.edu.iq
https://doi.org/10.24200/amecj.v8.i03.1087

elements, including soil, plants, water, and air. They can come from man-made (anthropogenic) sources such as energy production and metallurgy, sewage disposal, and agriculture (agrochemicals), or natural (geogenic) sources like parent rocks and minerals which exist naturally on the crust of Earth. For example, Southeast Asia's population has grown too quickly in recent decades, necessitating significant development of plans for industry and economy. Consequently, farmers use pesticides and fertilizers to meet the population's food needs, as well as untreated wastewater to irrigate the soil, which causes lead and cadmium to build up in the soil and food plants. Water is unquestionably a significant and essential component for maintaining life. It is the primary component of the lakes, rivers, and seas of Earth, as well as the liquids of the majority of organisms and the majority of living tissues. It makes up around 71% of the planet's surface. It also plays a significant role in the texture and processing methods of food and is a prominent component of all food kinds [2]. There are several ways that humans can be exposed to dangerous metals, including by eating or drinking tainted food or water, being around airborne particles, or using cutlery made of materials that could cause the minerals to seep into the food. Lead (Pb) is one of the most prevalent heavy metals that can be present in drinking water. It can replace calcium in bone and induce broad metabolic poisoning and enzyme inhibition. Adults may develop lead encephalopathy as a result of acute poisoning by organic lead compounds since lead compounds can also breach the blood-brain barrier in adults. The central nervous system, brain, kidney, hyperactivity, memory and concentration issues, high blood pressure, hearing issues, headaches, slowed growth, problems with reproduction in both men and women, digestive issues, and pain in the muscles and joints are all consequences of high lead levels in the body [3]. Cadmium is another significant metal (Cd). It has a lengthy biological half-life in the human body, ranging from 10 to 33 years, and is dangerous even at low concentrations. It can also build up in the body and ecosystems. Chronic exposures injure or impair the function of the central nervous system, the liver, and the kidneys. It is a global concern that developing nations lack adequate water supply systems and safe drinking water. Around 884 million people worldwide still do not get their drinking water from sources that have been certified, and nearly all of them live in poor nations. Many of the previous studies have addressed the treatment of heavy metal pollution. The different adsorbents and methods, such as DMP functionalized on MWCNTs and dispersive ionic liquid-suspension-micro-solid phase extraction (DILSMSPE), nanographene oxide(NGO) modified phenyl methanethiol nanomagnetic composite(Ph-CH_3SH), amine-functionalized bimodal mesoporous silica nanoparticles (NH2-UVM7) by ultrasound-assisted ionic liquid trap-micro solid phase extraction (USA-ILTMSPE), immobilization of 2-(aminomethyl) thiazole on MWCNTs, and functionalized bimodal mesoporous silica nanoparticles for efficient removal of lead in various matrices. [4-10].

This study aims to synthesize and characterize surface-modified magnetic chitosan nanocomposites and evaluate their efficiency in the removal of cadmium (Cd^{2+}) and lead (Pb^{2+}) ions from aqueous solutions using atomic absorption spectroscopy. The study also aims to optimize the adsorption conditions, assess the adsorption behavior through isotherm and kinetic models, and evaluate the thermodynamic parameters governing the adsorption processes.

2. Materials and Methods

2.1. Reagents and Materials

Chitosan with 80 mesh with a degree of deacetylation (75%–85%) from Merck (Germany), concentrated sulfuric acid (H_2SO_4, CAS No.:7664-93-9), hydrochloric acid (HCl, CAS No.: 7647-01-0, 36%), sodium hydroxide (NaOH, CAS No.: 1310-73-2), N,N′-dicyclohexylcarbodiimide (DCC, CAS No.: 538-75-0), $(NH_4)_2Fe(SO_4)_2.6H_2O$ and $FeCl_3$ were purchased from BDH, Ethylenediaminetetraacetic acid(EDTA, CAS No.: 6381-92-6) (99.0%) was also obtained

from Sigma-Aldrich, 3,3`-diaminobenzidine from sigma Aldrich, and the other materials were purchased from various commercial companies. All other reagents used in this study were analytical grade, and distilled or double-distilled water was used in the preparation of all solutions. Fourier-transform infrared spectroscopy (FTIR) of the prepared adsorbents was recorded by an FTIR-8101M Shimadzu spectrometer (Japan) with a KBr pellet in the region (400–4000 cm^{-1}) to investigate the chemical structures. The German (ALPHA II) device from the (BRUKER) company was also used to measure the prepared compounds. Adsorbent's structure and morphology were identified using an FEI NOVA NanoSEM 450 (Netherlands) field emission scanning electron microscopy (FESEM) under vacuum at an operating voltage of 10 kV. Patterns of X-ray diffraction (XRD) of the materials were recorded by a Rigaku X-ray powder diffraction diffractometer (Japan) using Cu Kα radiation with a wavelength of 1.54 Å at a scanning speed of 2 min^{-1} from 5°C to 80°C. Atomic Absorption Spectroscopy, Phoenix-986 (AA Spectrophotometer), Biotech Engineering Management Co., Ltd. Transmission Electron Microscopy (TEM) The specimen was measured using the AB912LEO. An FEI NOVA NanoSEM-450 is a Field Emission Scanning Electron Microscope (FESEM).

2.2. Preparation of chitosan@Fe_3O_4 composite (Ch@F)

The chitosan@Fe3O4 composite (Ch@F) was synthesized by the hydrothermal method [11]. In the first step, 0.5g chitosan was dissolved in dilute acidic distilled water (pH 5.5 by acetic acid). Chitosan solution was sonicated in 70 mL ethylene glycol. Subsequently, $FeCl_3$ (0.325g, 2.0mmol), $(NH_4)_2Fe(SO_4)_2.6H_2O$ (0.392g, 1.0mmol), ammonium hydroxide (15.0mL, 30%V/V), and sodium acetate (1.132g, 7.2 mmol) were mixed in the solution, which was then loaded into 100ml sealed Teflon container and placed in oven at 200^0C for six hours. Then, the mixture was cooled down to room temperature. After that, the mixture separates magnetically, then wash it with distilled water several times to get rid of the remaining ethylene glycol. The final solid material was dried to obtain Ch@F. The preparation was shown in Scheme 1.

2.3. Preparation of chitosan@EDTA@Fe_3O_4 composite (Ch@EDTA@F)

The Ch@EDTA composite was prepared according to the literature with some modifications [12]. 3.0 g of EDTA was dispersed in 50 mL of distilled water by ultrasonication for 3 hours. 2.0 g N,N´-dicyclohexylcarbodiimide (DCC) was added to the EDTA solution and stirred continuously for 2 hours to activate the carboxyl groups of EDTA [13]. The pH was maintained at 7.0 by a 2% NaOH solution. Then, the activated EDTA solution with 0.5 g Chitosan (Ch) was dispersed in 50 mL distilled water and 50 mL of 10% acetic acid by ultrasonication for 20min. After that, the solution was stirred at 60°C for an additional 3 hours. The precipitate after filtration was washed with 10% NaOH solution and distilled water in turn until the pH was 7.0. The obtained product Ch@EDTA@F was dried in a vacuum oven. The preparation was shown in Scheme 1.

2.4. Preparation of chitosan@EDTA@3,3´-Diaminobenzidine@Fe_3O_4 (Ch@EDTA@Am@F)

0.1g Ch@EDTA was sonicated for 3 hours in 50.0 mL of distilled water and 50.0 mL of 10% acetic acid. To activate the carboxyl groups of Ch@EDTA, 0.1g N,N´-dicyclohexylcarbodiimide (DCC) was added and constantly agitated for 2 hours while maintaining the pH at 7.0 with 2% sodium hydroxide. After that, the activated Ch@EDTA was mixed with 1.0 g of 3,3'-diaminobenzidine (Am) for 20 minutes under ultrasonication. The combined solutions were then agitated for a further 3 hours at 60°C. After filtering, the precipitate was rinsed with distilled water and then with a 10% NaOH solution until the pH reached 7.0. Finally, the Ch@EDTA@Am@F product was dried in a vacuum oven. The preparation was shown in Scheme 1.

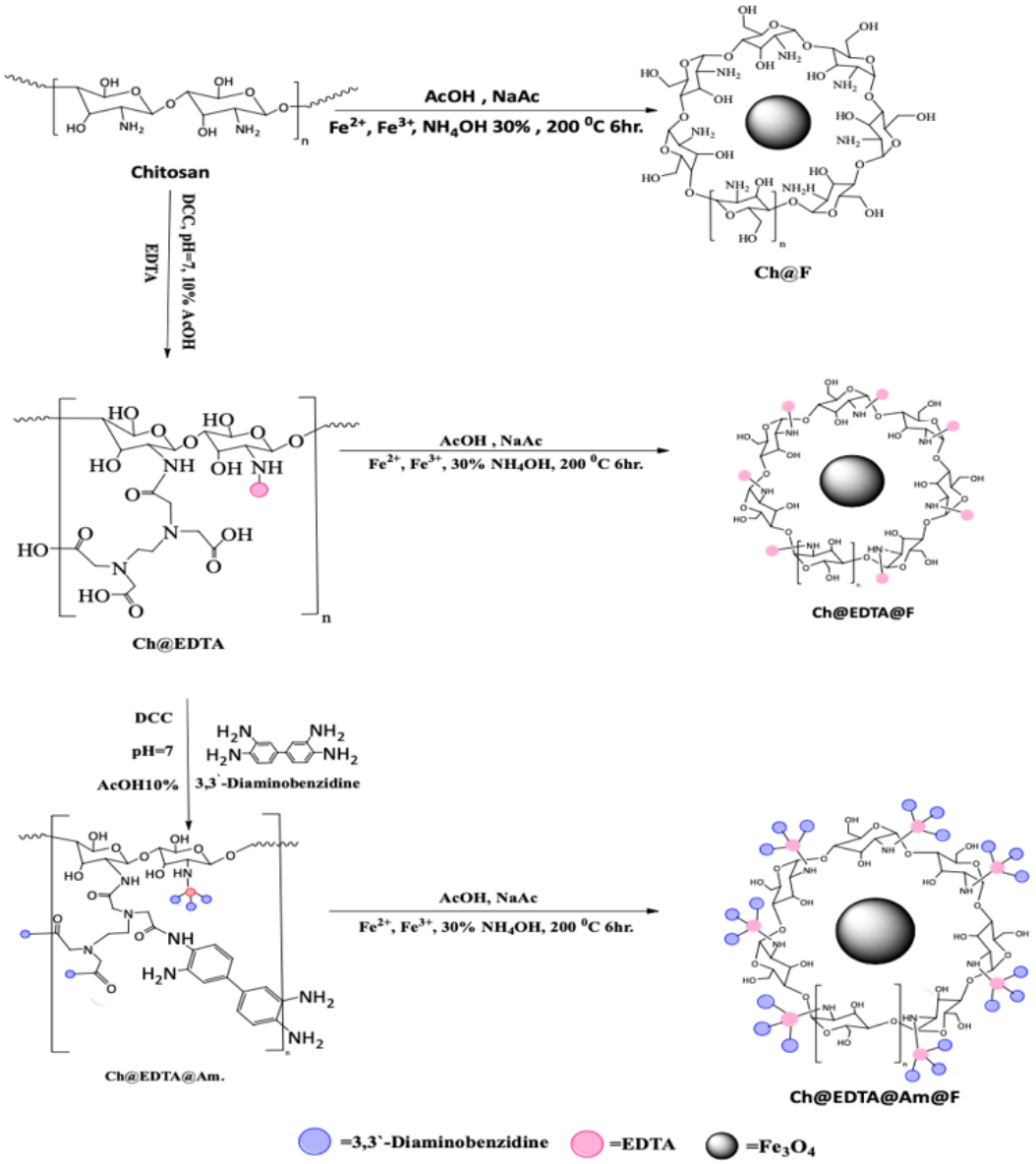

Scheme 1. Synthetic routes for preparing Ch@F, Ch@EDTA@F, and Ch@EDTA@Am@F

2.5. Preparation of cadmium and lead stock solutions

A standard solution of cadmium and lead 1000 mgL^{-1} was prepared for the adsorption experiments, and the required concentrations were obtained by dilution with distilled water.

2.6. General Procedure

Batch adsorption experiments [14-16] of cadmium and lead ions. were conducted in order to assess the adsorption characteristics and adsorption-influencing variables, the removing efficiency of synthesized adsorbents were examined by shaking 0.05g of each adsorbents with 50.0mL of ions solutions at initial concentrations, 50, 100, and 200 mg L^{-1} of cadmium ion and 100, 250, 400 mg L^{-1} of lead ion were an initial concentrations for Ch@F, Ch@EDTA@F, Ch@EDTA@Am@F adsorbents carried out on a thermostat shaker set to 27°C and 200 rpm for a predetermined amount of time. When the agitation time was complete, the adsorbents were separated magnetically from the solution, and the concentrations of remaining ions were determined with an atomic absorption

spectroscopy. The ion amounts on the adsorbents were evaluated using Equation 1.

$$q = \frac{(C_o - C_e)}{m} V \qquad \text{(Eq.1)}$$

Where C_0 and C_e (mg L^{-1}) are the initial and equilibrium concentrations of cadmium and lead ions in the solution, V (L) is the volume of metal ion solutions, m (in g) is the mass of the used adsorbents, and (in mg of ions per g of adsorbent) is the amount of adsorbed metal ions per gram of adsorbents (adsorption capacity). The adsorption isotherm studies were applied at optimum conditions including an agitation time of 6, 3 and 1 hour at pH 8.0 for cadmium ion and of 2, 1.5 and 1 hour at pH 5.0 for lead ion onto Ch@F, Ch@EDTA@F, and Ch@EDTA@Am@F respectively, with varying initial concentrations of cadmium ion (ranging from 50.0-200.0 mg L^{-1}) and (100-400 mg L^{-1}) for lead ion at constant temperature (27◦C). To study adsorption kinetics and to calculate enthalpy (ΔH°), entropy (Δ*S*°), and free energy (ΔG°), the experiments were conducted at 27°C, 40°C, and 55°C, with 0.05 g of adsorbents. After the absorption of Cd and Pb with adsorbents in 50 mL of solution, it was back-extracted with nitric acid (5 mL, 0.5 M) and determined by flame atomic absorption spectrometry (F-AAS). LODs of 3.3 μgL^{-1} for Pb and 0.58 μgL^{-1} for Cd were obtained. After preconcentration (PF=10), the linear ranges of cadmium are 2–300 μg L^{-1}, and Pb is 10–1500 μgL^{-1}.

3. Results and Discussion

3.1. FTIR characterization

The FTIR spectra showed the characteristic bands of the Ch@F shown in Figure 1a. The band at 3353 cm^{-1} corresponds to the O-H bond stretching vibration. The peak at 538 cm^{-1} represented the Fe–O groups. Figure 1b shows the characteristic bands of Ch@EDTA at 1674 cm^{-1} and 1593 cm^{-1}, assigned to C=O stretching vibrations. These results confirmed the presence of the amino group Ch with EDTA through an amide bond. Moreover, the strong characteristic appearing at 1427 cm^{-1} can be assigned to the C-O vibration of the COO group, which suggests the existence of the carboxyl group of EDTA modified on chitosan. The broad band at 3217-3447 cm^{-1} corresponds to the O-H of carboxylic acid [17]. The appearance of the peaks at 1622, 1486, and 1083 cm^{-1} assigned to the symmetrical stretching vibration of C=O, C-N in amides, and stretching vibration of C-N in amines, respectively, as shown in Figure 1c, indicates a successful reaction between Ch@EDTA and Am (amine groups) [18]. The strong broad band at 3329-3448 cm^{-1} (O-H stretching vibration in EDTA carboxylic functional groups) became sharper and is shifted to 3165-3359 cm^{-1} after the reaction with Am, due to the removal of O-H in carboxylic groups and the formation of amide groups [19]. It can be seen that Ch@EDTA@F and Ch@EDTA@Am@F display the characteristic absorption of Fe-O stretching vibrations at 539cm^{-1} and 546cm^{-1}. As shown in Figure 1d, 1e respectively.

3.2. High-Resolution Transmission Electron Microscopy (HRTEM)

High-resolution transmission electron microscopy (HRTEM) is the most common technique to analyze nanoparticle size and shape, since it provides not only direct images of the sample but also the most accurate estimation of the nanoparticle homogeneity. The main advantage of this approach is its fantastic capacity to penetrate the sample with an electron beam, allowing for a thorough examination of its internal structure. Figure 2 observes clear morphological changes of nanocomposites. Magnetite nanoparticles are widely distributed on the surface of the matrix. Furthermore, Fe_3O_4 NPs are well wrapped by the shell layer. The shell is adsorbed by electrostatic and hydrogen bonding to the surface of the magnetite. Transmission electron microscopy of the as-synthesized MNPs shows a median size of nm, indicating that they have a spherical or multidimensional shape (N =18.4), which was calculated by the ImageJ program. The selective area electron diffraction (SAED) also indicated the crystalline structure of Fe_3O_4 nanoparticles

depicted in Figure 2. The dark field revealed a single crystal structure of Fe_3O_4 nanoparticle. The image exhibits well-defined and distinct lattice fringes, which can be attributed to the Miller indices and corresponding interplanar spacings of the (1 1 1), (2 2 0), (3 1 1), (4 0 0), (5 1 1), and (4 4 0) planes, indicate that the NPs are highly poly crystalline.

3.3. Energy Dispersive X-ray Spectroscopy

The presence of elements in the structures of compounds was investigated using X-ray energy dispersive spectroscopy (EDX) analysis. The elemental analysis of the nano composite by EDS revealed the presence of Fe, O, H, C, and N as the only components of the particles, as shown in Figure 3.

3.4. High-Resolution Scanning Electron Microscopy (HRSEM):

The field emission scanning electron microscope (HRSEM) is an essential technique for examining the studied surfaces, as it provides details about the shape of the particles and the nature of the aggregation between them, as well as the nature of the surfaces in terms of whether they are porous or smooth, as well as determining the degree of homogeneity between the components and their distribution on the surface. SEM analysis has been used to validate the morphology of pure Fe_3O_4 nanoparticles and modified nanocomposites presented in Figures 4-6. The SEM images unequivocally demonstrate that the Fe_3O_4 nanoparticles possess a spherical shape and confirm the success of the coating process on the surface of Fe_3O_4 particles with a good distribution. The images also showed that there was agglomeration in the prepared compounds and that the surfaces of the compounds contain many pores or holes. Since these pores will increase the surface area of the compounds, it is expected that these holes will play an essential role in enhancing the adsorption process of heavy elements on the surface of the adsorbent materials.

3.5. X-ray Diffraction Spectroscopy (XRD)

Technology for X-ray diffraction (XRD) is a crucial diagnostic tool for nanoparticles and nanocomposites. Additionally, X-ray diffraction (XRD) is a quick and non-destructive analytical technique that frequently yields precise results for identifying samples [20]. XRD analysis, as shown in Figure 7, verifies that the produced MNPs are predominantly composed of magnetite. The obtained patterns displayed a high level of agreement with the data from the reference database of magnetite (JCPDS card No. 19-0629) [17]. Notably, the as-synthesized samples exhibit excellent crystallinity with well-defined magnetite peaks, showcasing the high quality of these particles. The peaks can be indexed at the values of 2θ = 30.2° (220); 35.4° (311); 43.4° (400); 53.9° (422); 56.9° (511); and 62.6° (440), respectively, for the MNP-Fe_3O_4. The inclusion of chitosan also caused a broad peak in the Chm patterns at 2θ = 20.3°. The results suggest that the synthesized Fe_3O_4 the particles have homogeneous morphological properties and a high degree of crystallinity. These diffraction patterns are consistent with the calculated X-ray diffraction patterns reported in the literature [17]. The average crystallite size, D (nm), of the studied materials was calculated using the Debye–Scherrer Equation 2 [21].

$$D = \frac{K_s \,.\, \lambda}{\beta . cos\theta} \qquad \text{(Eq.2)}$$

Where D was the size of the crystal, λ was the wavelength for X-ray diffraction in (nm) for CuKα1, which is equivalent to 1.54060 Å translated to 0.154nm, and Ks is the constant, usually written as 0.9, which is related to the crystal structure's shape. The Full Width Half Maximum (FWHM) of spherical crystals with cubic unit cells in radian angle units is represented by β. This can be derived from each graph after converting each compound's X-ray diffraction spectroscopy to radian angle. As a result, the 2θ was divided by two and then multiplied by 0.01745329 to become θ. Furthermore, β was determined using the relationship [22] that follows: 1 Degree = 0.01745329 radians, θ in radian angle = (2θ/2x0.01745329), β = Value of FWHM x 0.01745329.

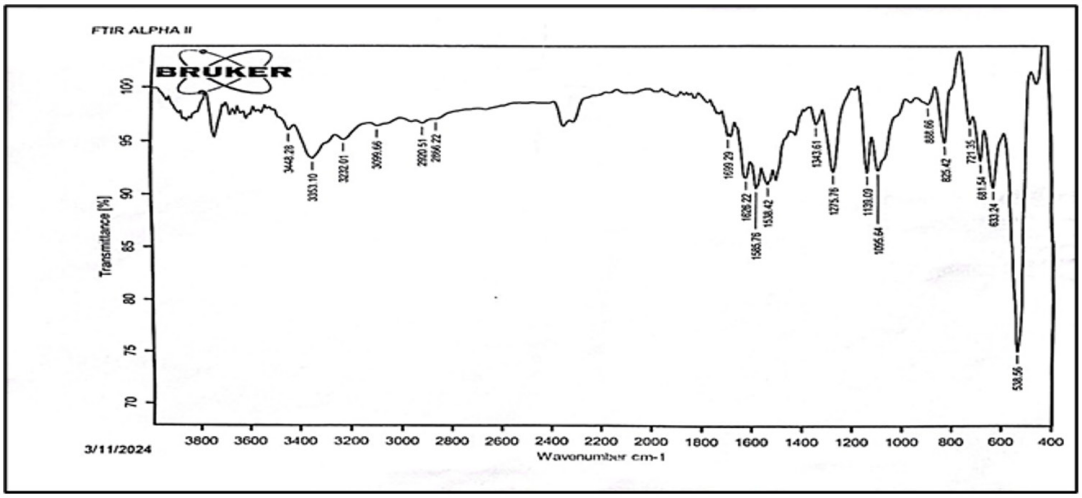

Fig. 1a. FTIR spectra of Ch@F adsorbent

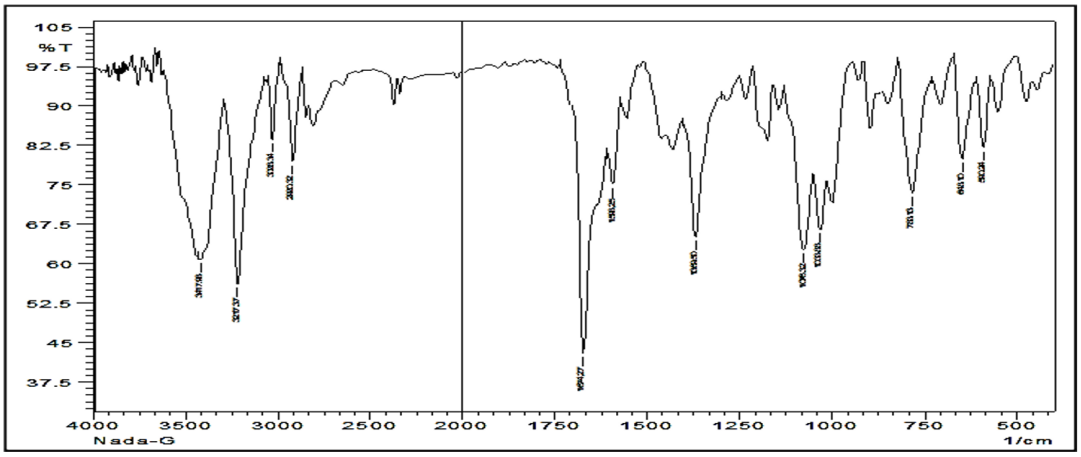

Fig. 1b. FTIR spectra of Ch@EDTA adsorbent

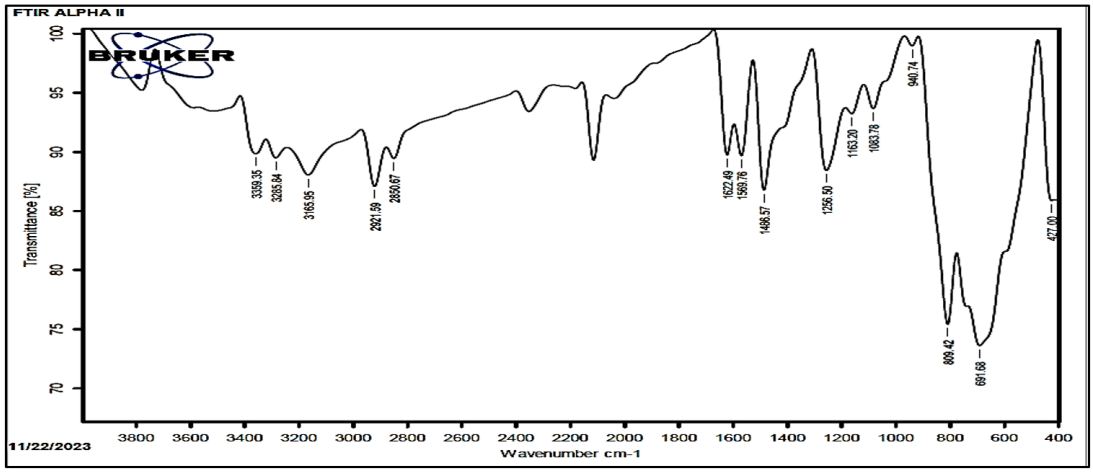

Fig. 1c. FTIR spectra of Ch@EDTA@Am adsorbent

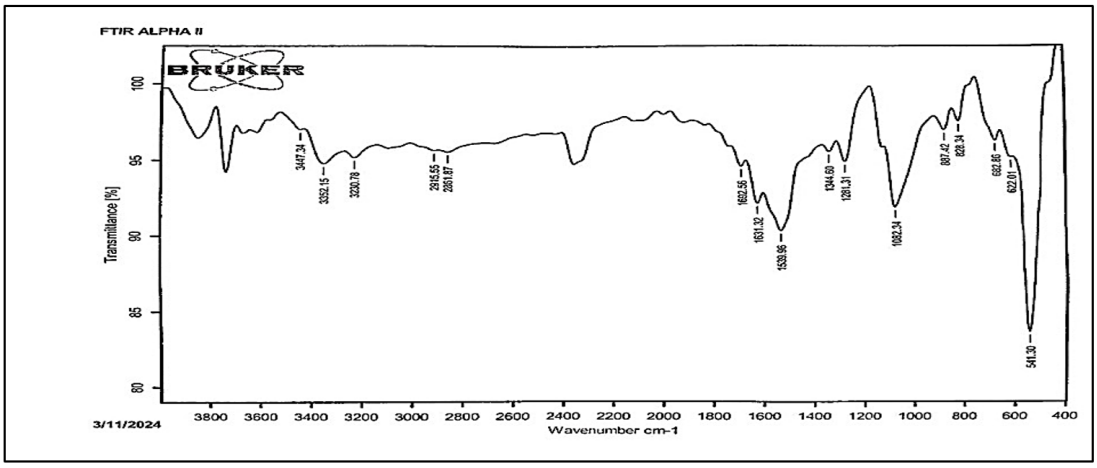

Fig. 1d. FTIR spectra of Ch@EDTA@F adsorbent

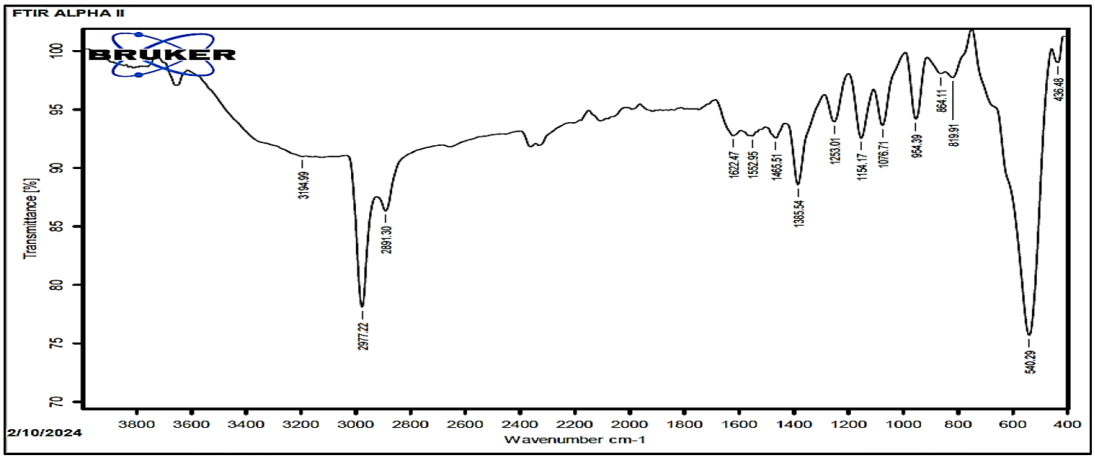

Fig. 1e. FTIR spectra of Ch@EDTA@Am@F adsorbent

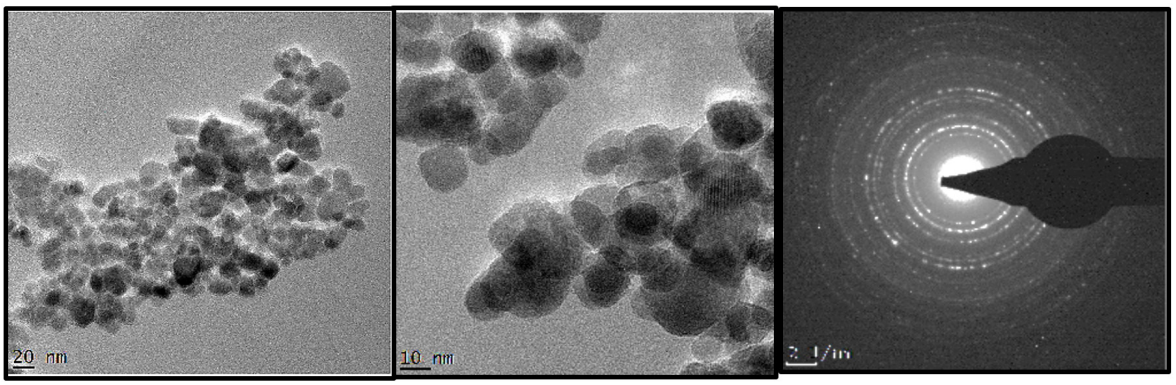

Fig. 2. HRTEM images of Ch@EDTA@Am@F adsorbent

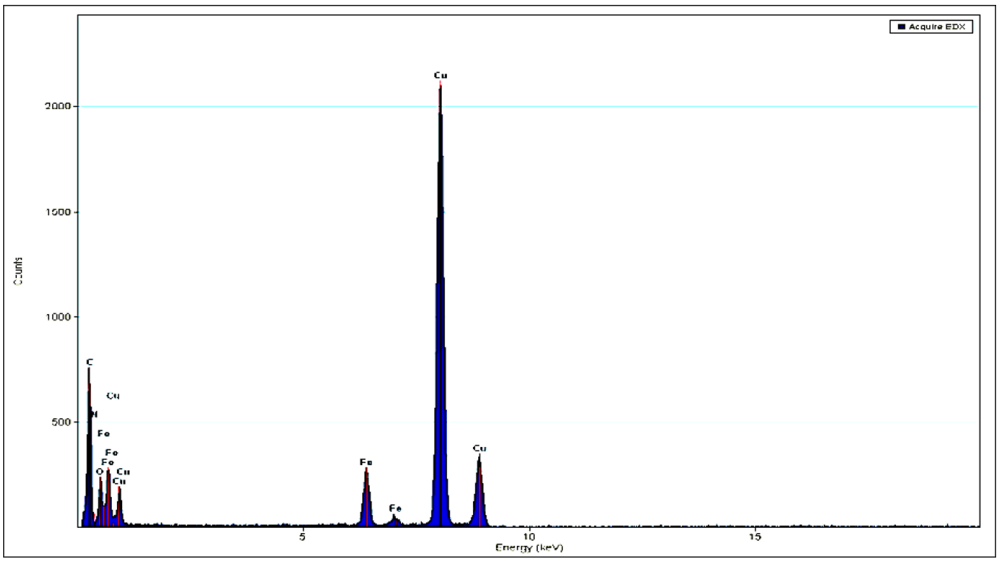

Fig. 3. EDX of Ch@EDTA@Am@F adsorbent

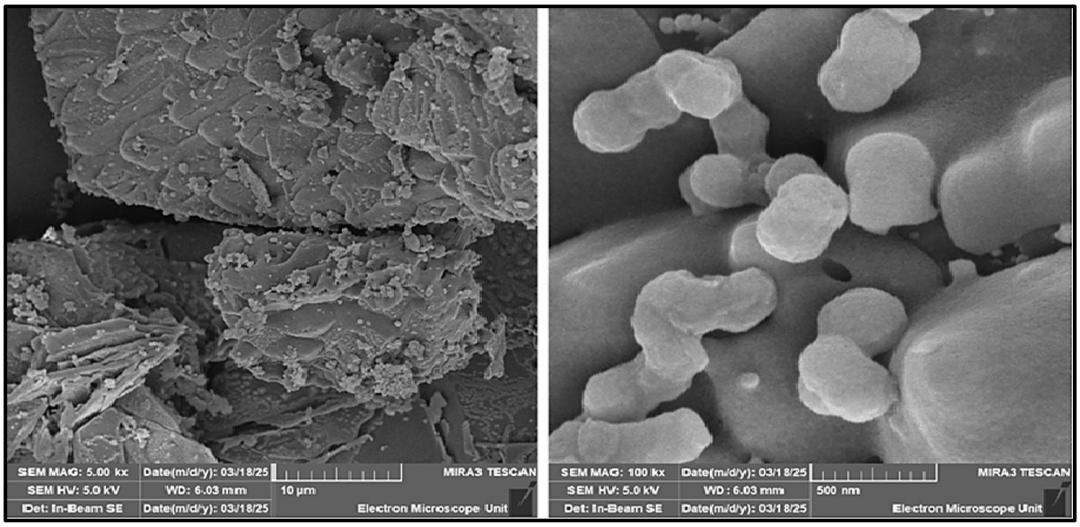

Fig. 4. HRSEM images of Ch@F adsorbent

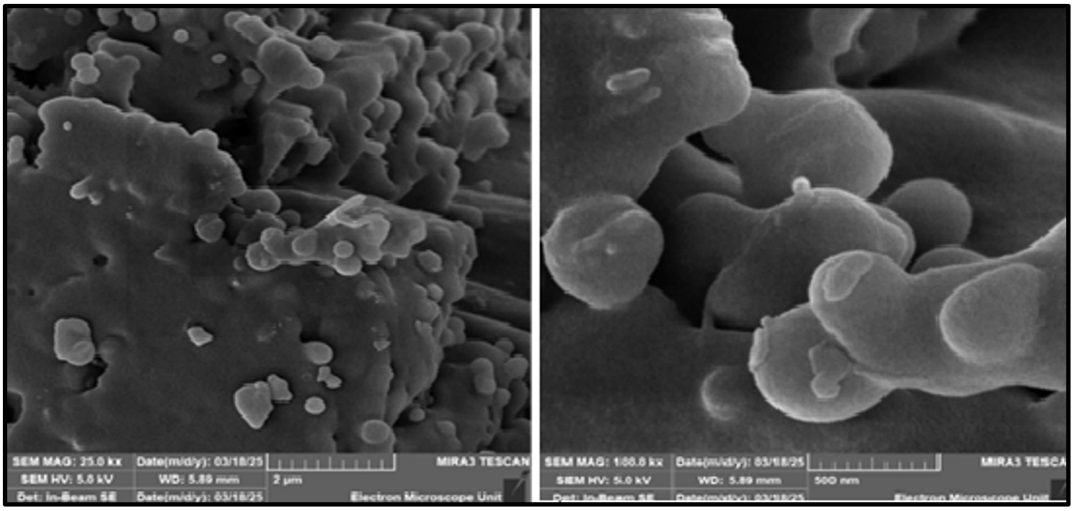

Fig. 5. HRSEM images of Ch@EDTA@F adsorbent

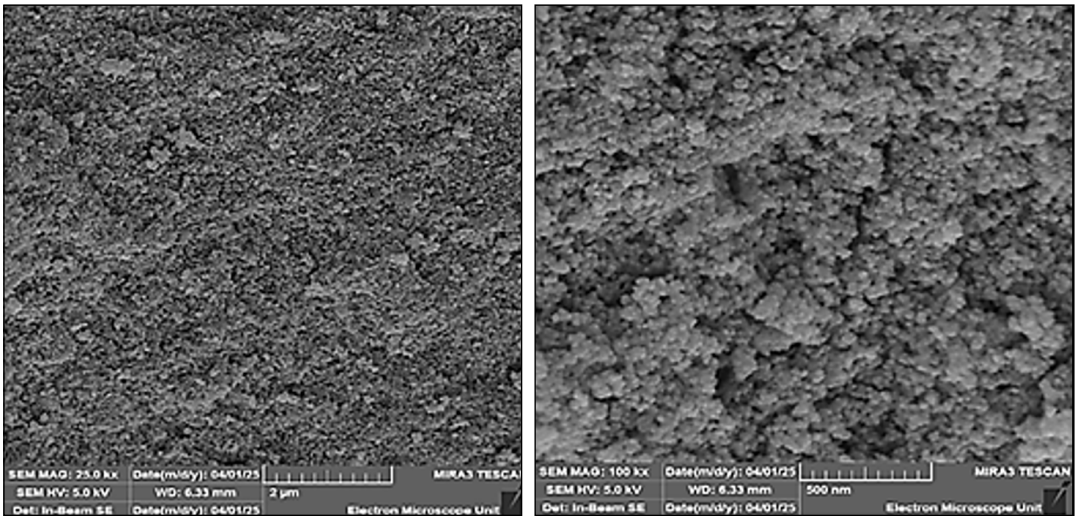

Fig. 6. HRSEM images of Ch@EDTA@Am@F adsorbent

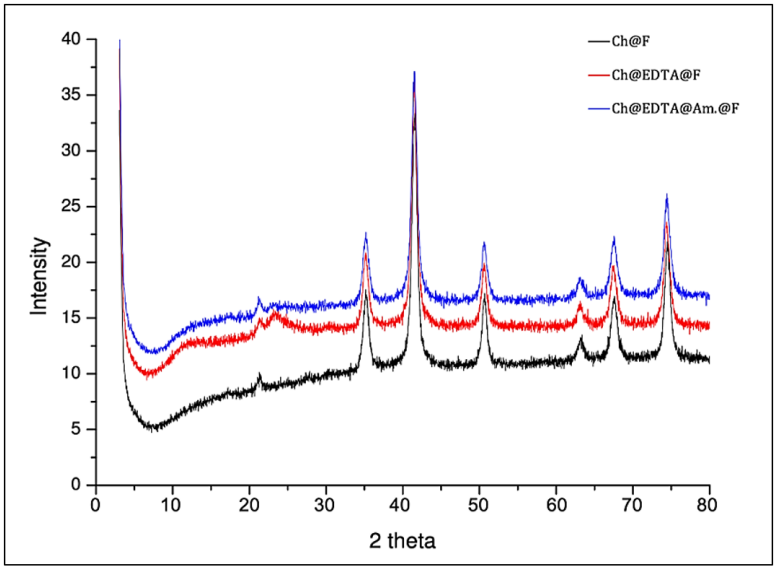

Fig. 7. XRD of Ch@F, Ch@EDTA@F, and Ch@EDTA@Am@F adsorbents

3.6. Optimization of cadmium and lead ions adsorption

The batch systems were employed in adsorption experiments of cadmium and lead ions aqueous solutions, and the adsorption efficiencies were evaluated with respect to optimum pH, contact time, temperature, and the initial concentration (C_0).

3.6.1.Effect of pH

The effect of pH on the adsorption capacities of all adsorbents, as shown in Figure 8 (a and b), was studied at different values ranging from 2.0 to 8.0 for cadmium and from 2.0 to 5.0 for lead because they precipitated as metal hydroxide above these values. Figures 8a and 8b show that the adsorption capacities were increasing gradually with pH increasing, at a strong acidic media there were an abundance of H^+ ions which compete cadmium and lead ions towards adsorbents surface resulting in decreasing the adsorption capacity, but when the pH increased the loading of cadmium and lead ions be more favorable, on the other hand a the elevation of pH values of the solution lead to a decrease in the solubility of ions, and ultimately leads to achieving maximum efficiency and adsorption capacity [23, 24].

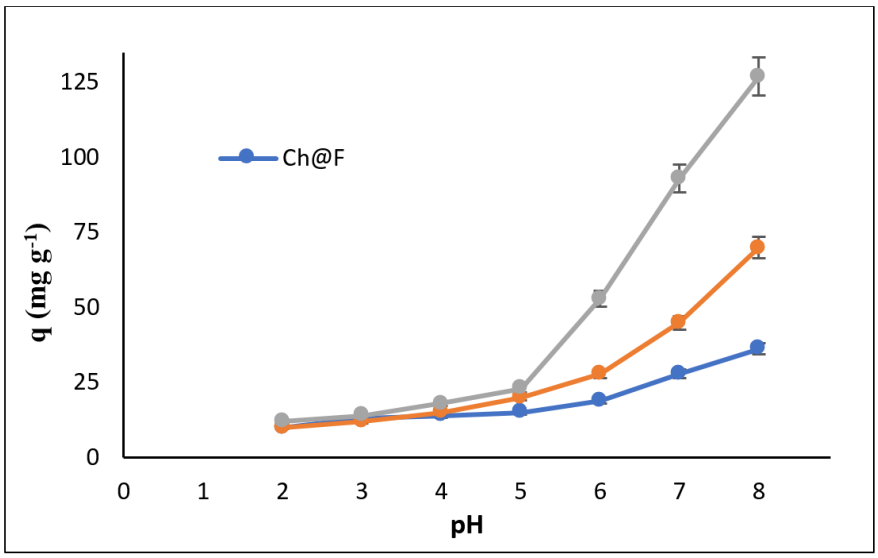

Fig. 8a. Effect of pH for cadmium ion solution at 27 °C

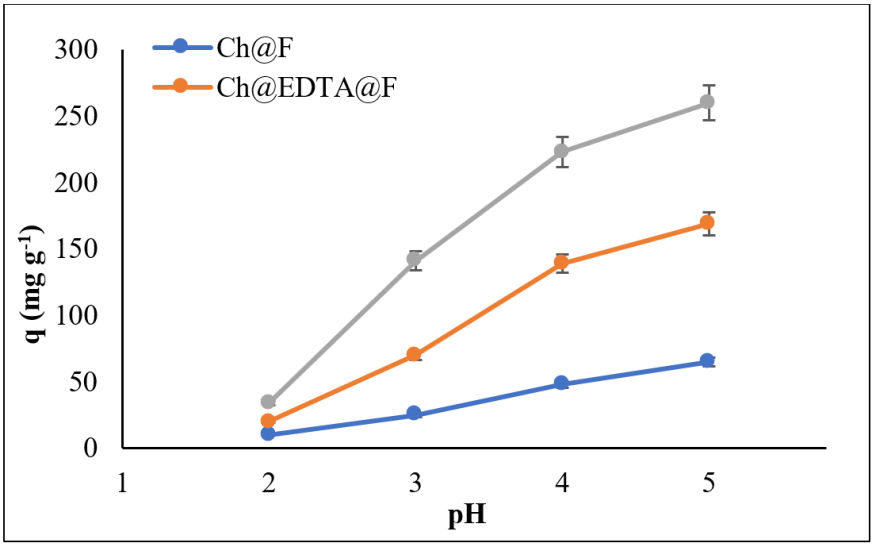

Fig. 8b. Effect of pH for lead ion solution at 27 °C

3.6.2.Effects of Agitation Time and Temperature on the Adsorption

One of the most crucial factors in the adsorption process is the effect of the contact time between the adsorbent and the adsorbate, since determining the equilibrium contact time is critical in predicting the viability and performance of an adsorbent for a process [25]. The effect of contact time on the adsorption of cadmium ions onto Ch@F, Ch@EDTA@F, and Ch@EDTA@Am.@F was studied at different temperatures, 27, 40, and 55 °C. The Figures 9 (A, B, C) and Figures10 (A, B,C) show the adsorption efficiencies of cadmium and lead ions had increased rapidly from low agitation time until reach an equilibrium at all temperatures, the results indicated that the equilibrium agitation times for cadmium were 6, 3 and 1 hours and for lead were 2, 1.5 and 1 hours for Ch@F, Ch@EDTA@F, and Ch@EDTA@Am@F, respectively.

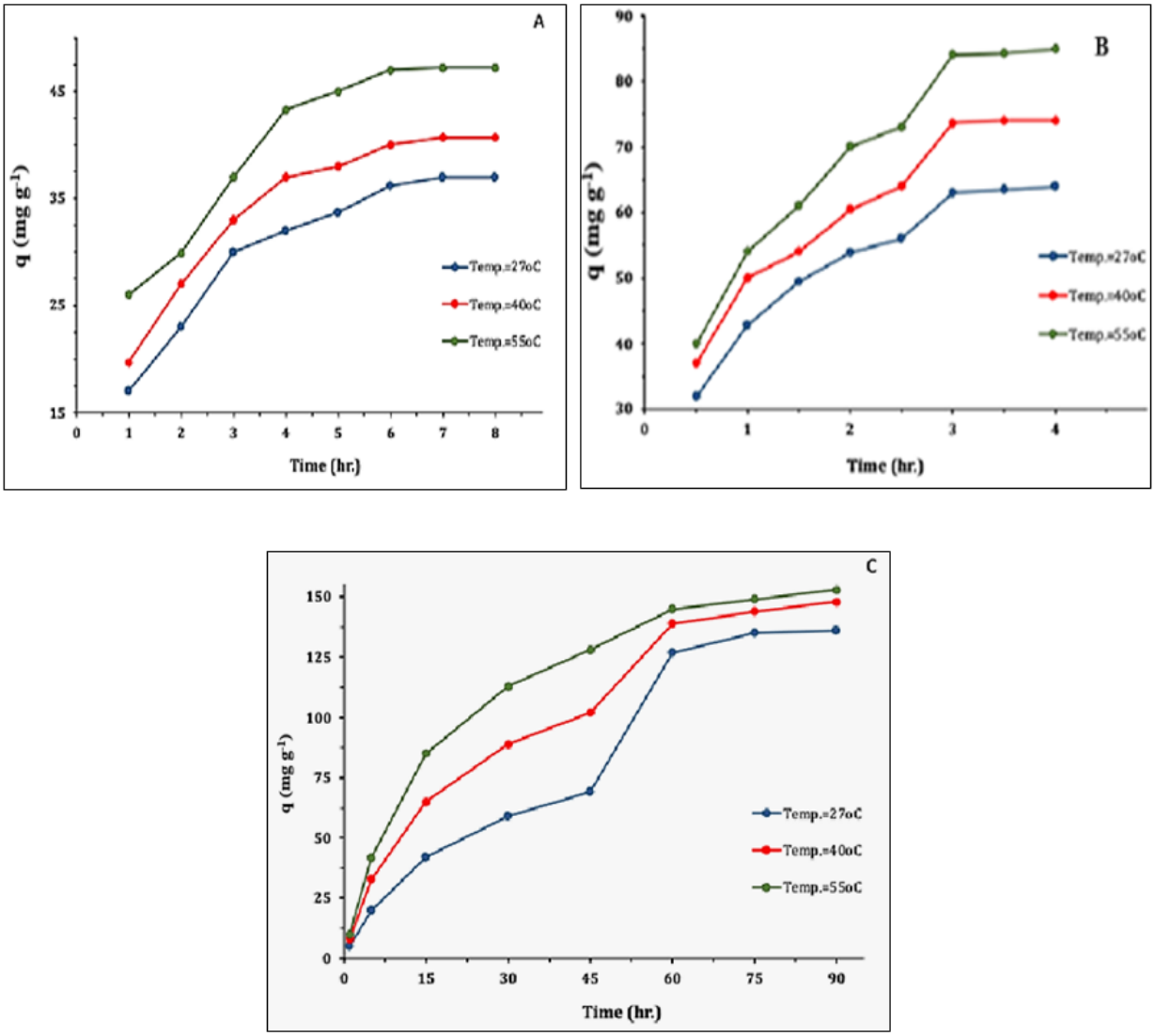

Fig. 9. Effect of Agitation time for Cadmium ion onto (A) Ch@F, (B) Ch@EDTA@F, (C) Ch@EDTA@Am.@F at 27 °C, 40 °C, and 55 °C.

3.7. Adsorption isotherms

The equilibrium relationship and interaction between the adsorbent and adsorbate at a certain temperature are shown by the adsorption isotherms. Finding the best-fitting isotherms to explain the adsorption process is essential [26]. The adsorption isotherms were examined in order to establish a basis for determining adsorption capacity, exposing adsorption behavior, and proposing potential adsorption mechanisms [27]. Several isotherm models could be used to describe the experimental data of adsorption models and were applied to the obtained equilibrium data. In this study, Langmuir [28,29], Freundlich [30], Temkin [31,32], and Dubinin–Radushkevich [33,34] models were used. According to the Langmuir model, a monolayer covering of adsorbate molecules forms on a uniform adsorbent surface without any interaction between the molecules. The most widely used isothermal adsorption model has shown strong agreement with a number of experimental data [28, 29]. The Langmuir model's linearized form is provided in Equation 3.

$$\frac{C_e}{q_e} = \frac{1}{q_{max} K_L} + \frac{C_e}{q_{max}} \qquad \text{(Eq.3)}$$

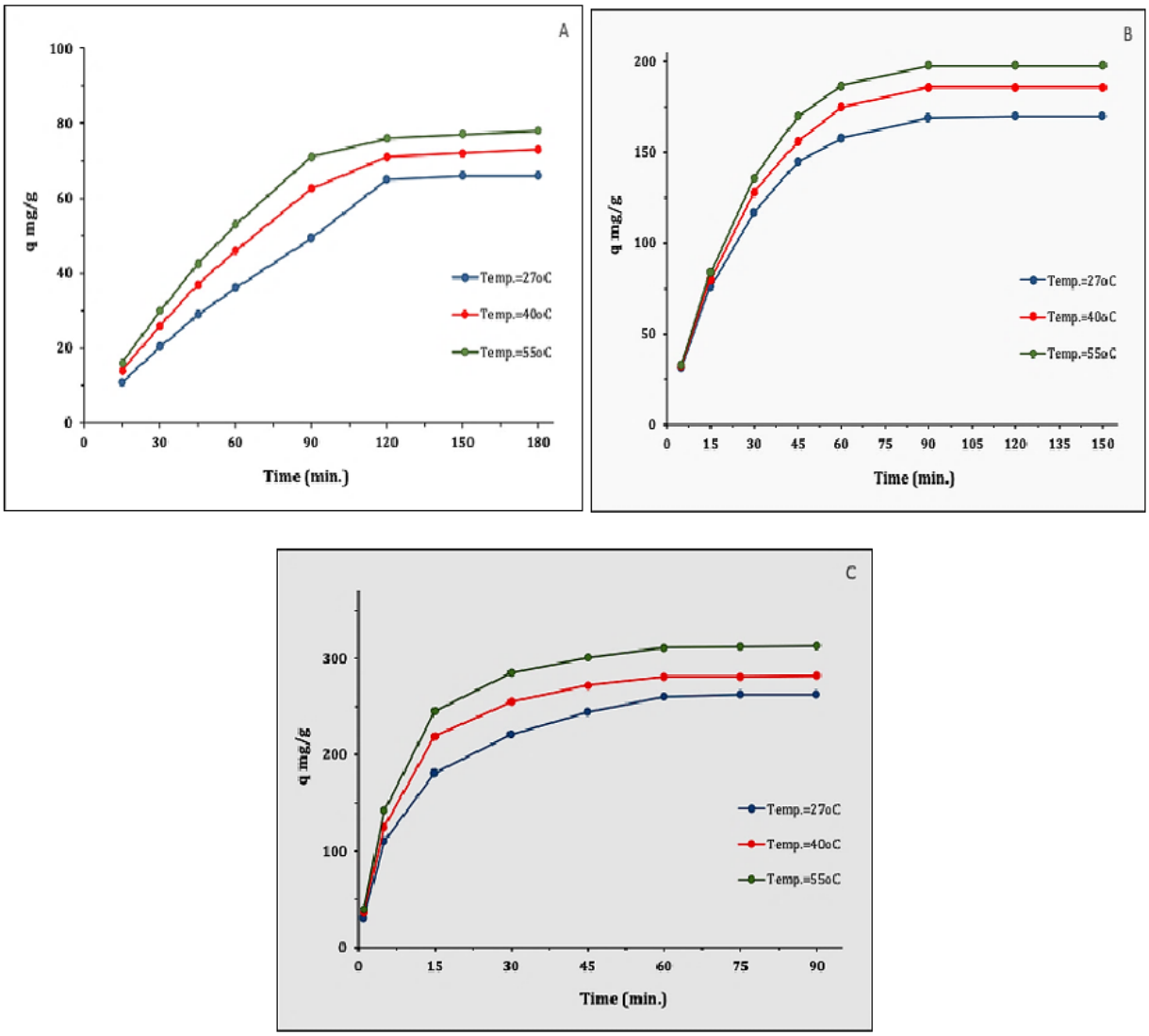

Fig. 10. Effect of Agitation time for Lead ion onto (A): Ch@F, (B): Ch@EDTA@F, (C): Ch@EDTA@Am@F at 27 °C, 40 °C, and 55 °C

where q_e is the amount adsorbed, C_e is the equilibrium concentration, q_{max} the maximum adsorption capacity reflected on a complete monolayer, and K_L represents the Langmuir constant that is related to the apparent energy of adsorption. Equation 4 [35] defines the separation factor or equilibrium parameter (R_L), which can be used to characterize the key features of the Langmuir isotherms:

$$R_L = \frac{1}{1+K_L C_e} \qquad \text{(Eq.4)}$$

where R_L values indicate the type of adsorption to be irreversible ($R_L = 0$), favorable ($0 < R_L < 1$), linear (RL = 1), or unfavorable ($R_L > 1$). This model is the most commonly used isothermal adsorption model and has demonstrated good agreement with various experimental data [28,29]. Figure 11 (A, B) shows the plots of the Langmuir adsorption isotherms of cadmium and lead adsorbed onto Ch@F, Ch@EDTA@F, and Ch@EDTA@Am@F, respectively. Table 1 displays q_{max}, K_L, R_L, and the correlation coefficient R^2 results for the Langmuir isotherms. The calculated R_L values were found to be equal (0.1638, 0.16553, and 0.70872) for

cadmium and (0.62755, 0.62092, and 0.82847) for lead by Ch@F, Ch@EDTA@F, and Ch@EDTA@Am@F, respectively. Under the imposed ideal condition, the computed results demonstrated that all adsorbents were advantageous for adsorbing metal ions from solutions. Freundlich adsorption isotherm is an empirical equation that is widely used for the adsorption equilibrium explanation [30], which is based on adsorption on the surface of a heterogeneous multilayer, and assumes that the adsorption takes place at sites with varying energy of adsorption [36]. The Freundlich isotherm is represented in Equation 5 [37].

$$lnq_e = lnK_F + \frac{1}{n} lnC_e \qquad \text{(Eq.5)}$$

Where K_F and n, respectively, are Freundlich constants associated with adsorption intensity and capacity. The n-value is a measure of the degree of surface heterogeneity, which characterizes the distribution of the adsorbed molecules on the adsorbent surface, and the K_F shows the adsorption capacity of the adsorbent toward the adsorbate. Figure 12 (A,B) represents the Freundlich adsorption isotherms plots of cadmium and lead ions onto Ch@F, Ch@EDTA@F, and Ch@EDTA@Am@F. Table 2 displays Freundlich isotherm constants K_F, 1/n, and the correlation coefficient R^2, which were determined from the plot of *ln* q_e against ln C_e, the slope of and intercept K_F. The adsorbent's ability to adsorb the adsorbate is indicated by the Freundlich constant, or K_F. A greater affinity for the adsorbate is indicated by a higher K_F value [38]. Generally speaking, the adsorption capacity of the specified adsorbent rises in tandem with the K_F values [39]. According to the results, K_F indicated that all as-synthesized adsorbents had a higher affinity for lead and cadmium ions. The 1/n is the adsorption intensity, and its magnitude is an indicator of the favorability of adsorption. In general, the value of 1/n gives an idea about the type of isotherm, whether it is irreversible (1/n=0), favorable (0 < 1/n < 1), or unfavorable (1/n > 1) [40]. It can be noticed from Table 2 that all the values of 1/n are less than 1, demonstrating that it is favorable for chemisorption for all adsorption systems of cadmium and lead ions [41]. The nature of the adsorption, including its chemical or physical character, is examined via the Dubinin–Radushkevich (D-R) isotherm [42]. The linear form of the D-R isotherm model was given by Equation 6 [33,34].

$$lnq_e = lnq_{max} + K_D\varepsilon^2 \qquad \text{(Eq.6)}$$

Where q_e, and q_{max} are the equilibrium adsorption capacity and the maximum adsorption capacity under optimized conditions in the D-R isotherm model, respectively; K_D is a constant related to the mean adsorption energy (E_D), and ε is the Polanyi potential, which is associated with the equilibrium concentration, which is given by Equation 7.

$$\varepsilon = R\,T\,ln\left(1 + \frac{1}{C_e}\right) \qquad \text{(Eq.7)}$$

The mean free energy E_D of adsorption per molecule of adsorbate (for removing a molecule from its location in the sorption space to infinity in the solution) can be calculated using Equation 8.

$$E_D = \frac{1}{2K^{1/2}} \qquad \text{(Eq.8)}$$

Figure 13 (A, B) shows plots of the D-R adsorption isotherms of cadmium and lead ions onto Ch@F, Ch@EDTA@F, and Ch@EDTA@Am.@F. Table 3 presents the values of D-R isotherm parameters q_{max}, K_D, E_D, and R^2, which were determined from the linear plot of *ln* q_e versus ε^2; the slope and intercept of the plot give KD and qmax values, respectively. Moreover, the D-R model can reveal the adsorption type (physical or chemical adsorption) according to the mean free energy of adsorption (E_D). Generally

speaking, when the E_D is less than 8 kJ·mol-1, physical adsorption predominates, whereas when the E_D is greater than 8.0 kJ mol^{-1}, chemical adsorption takes the lead [43]. The E_D values exceeded 8.0 kJ mol^{-1}, indicating that chemical interactions dominate the adsorption of lead and cadmium ions onto the produced adsorbent. According to the Temkin isotherm, adsorption is defined by a uniform distribution of binding energies up to a specific maximum binding energy, and the heat of adsorption of all molecules in a layer decreases linearly with coverage as a result of adsorbent-adsorbate interactions [31, 32]. Equation 9 of the Temkin isotherm can be expressed in a linear form [44].

$$q_e = B_T ln A_T + B_T ln C_e \qquad \text{(Eq.9)}$$

Where B_T, Temkin constant equal to RT/bT, T (in K^0) is absolute temperature, R equal to 8.314 J mol^{-1} K^{-1} is the universal gas constant, bT (in kJ.mol-1) is related to the heat of adsorption, and AT (in L.mg-1) is the equilibrium constant corresponding to the maximum binding energy. A plots of q_e versus lnC_e for the Temkin model are shown in Figure 14 (A, B) for the adsorption of cadmium and lead ions onto as-prepared adsorbents. Also, Temkin isotherm parameters for the adsorption of cadmium and lead ions onto adsorbents showed in Table 4. Table 1 shows that the Langmuir isotherm model was more fitted than the Freundlich, Dubinin–Radushkevich, and Temkin models for removing cadmium and lead by all adsorbents, where the intricacy of adsorption processes was inspired. However, it might be said that there was a propensity for chemical adsorption to occur between metal ions and the functional groups of adsorbents.

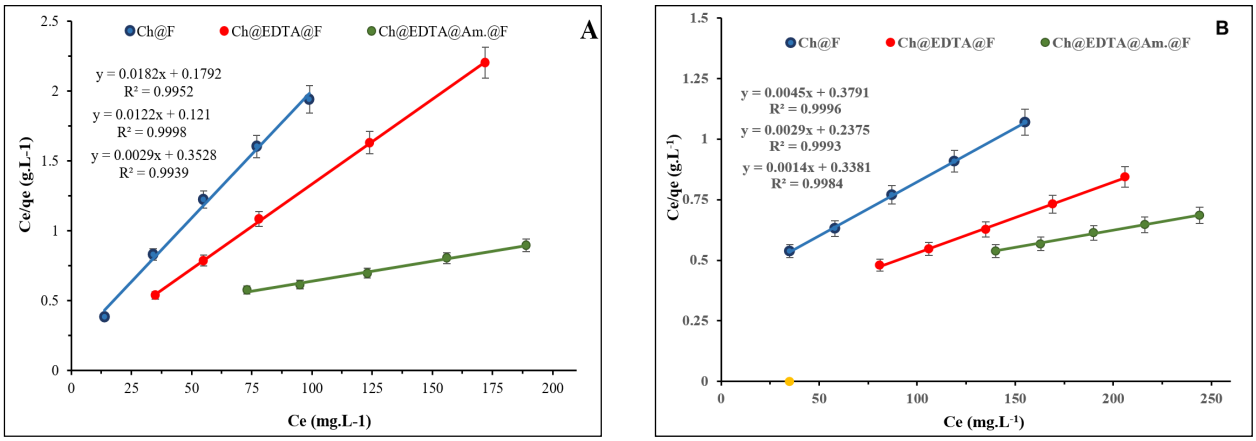

Fig. 11. Langmuir isotherm model for (A): Cadmium (B): Lead ion solution at 27°C

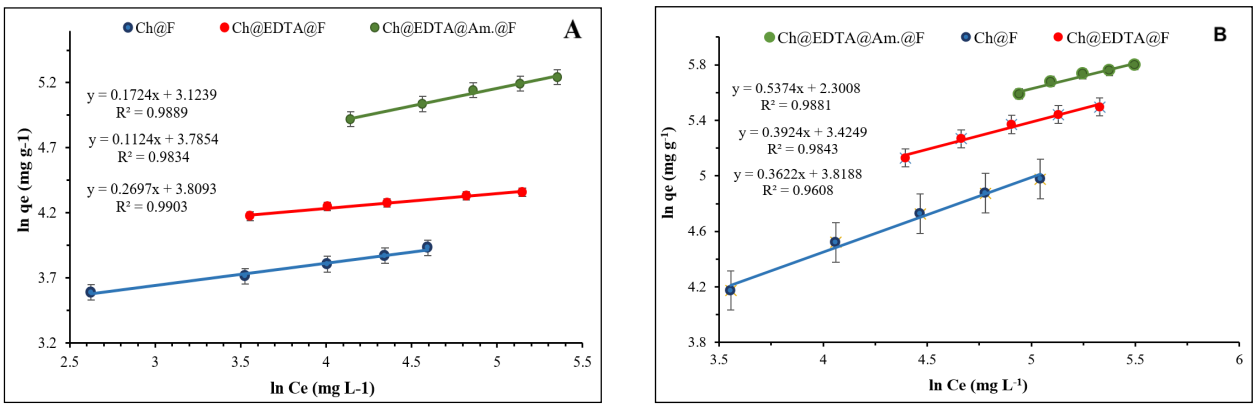

Fig. 12. Freundlich isotherm model for (A): Cadmium (B): Lead ion solution pH at 27 °C

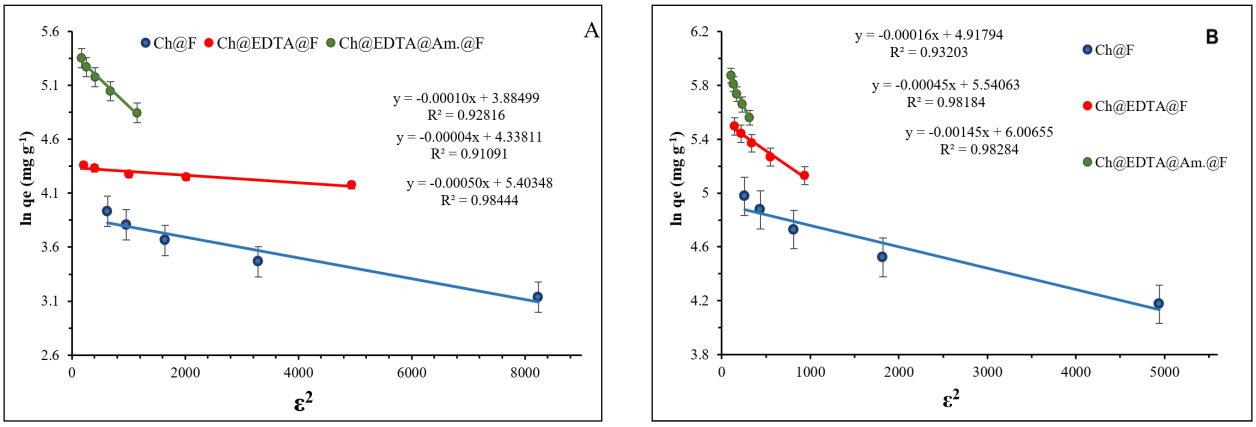

Fig. 13. D-R isotherm model for (A): Cadmium (B): Lead ion solution at 27°C

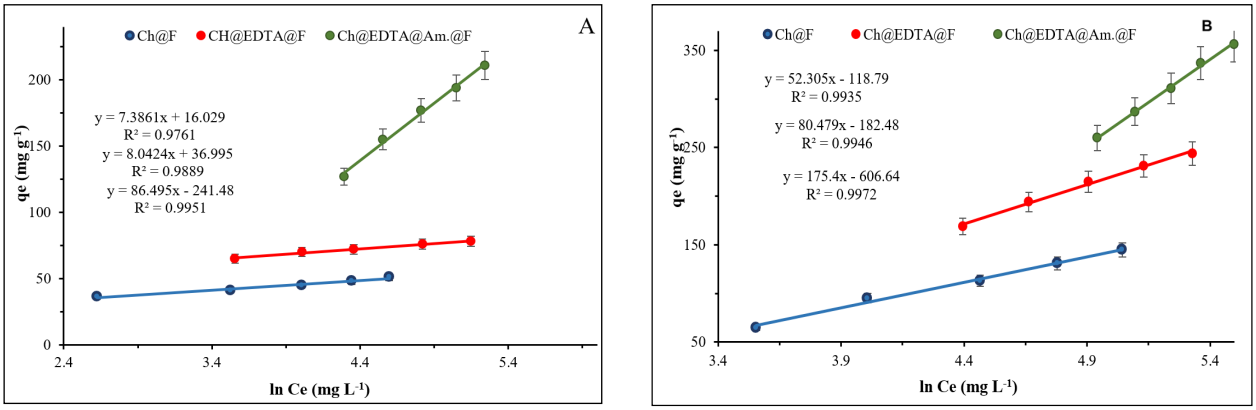

Fig.14. Temkin isotherm model for (A): Cadmium (B): Lead ion solution pH at 27°C

Table 1. Langmuir isotherm parameters for the adsorption of cadmium and lead ions onto adsorbents

Adsorbent	Cadmium				Lead			
	q_{max}	K_L	R_L	R^2	q_{max}	K_L	R_L	R^2
Ch@F	54.64	0.10212	0.1638	0.9952	222.2	0.0119	0.6276	0.9952
Ch@EDTA@F	81.97	0.10083	0.1655	0.9998	344.8	0.0122	0.6209	0.9993
Ch@EDTA@Am@F	344.8	0.0082	0.7087	0.9939	714.3	0.0041	0.8285	0.9984

q_{max} (mg g^{-1}), k (Lmg^{-1})

Table 2. Freundlich isotherm parameters for the adsorption of cadmium and lead ions onto adsorbents

Adsorbent	Cadmium				Lead			
	K_F	1/n	R^2	K_F	1/n	R^2	R_L	R^2
Ch@F	22.735	0.1724	0.9889	9.9822	0.5374	0.9881	0.6276	0.9952
Ch@EDTA@F	44.053	0.1124	0.9834	30.72	0.3924	0.9843	0.6209	0.9993
Ch@EDTA@Am@F	14.092	0.5201	0.9804	16.366	0.5608	0.9983	0.8285	0.9984

K_F (L mg^{-1})

Table 3. D-R isotherm parameters for the adsorption of cadmium and lead ions onto adsorbents

Adsorbent	Cadmium				Lead			
	q_{max}	K_D	E_D	R^2	q_{max}	K_D	E_D	R^2
Ch@F	48.667	0.0001	70.71	0.9289	136.715	0.00016	55.9	0.9289
Ch@EDTA@F	76.562	3.5E-05	119.5	0.9109	254.838	4.5E-05	105.4	0.9818
Ch@EDTA@Am.@F	222.183	0.000499	31.65	0.9844	406.019	0.001452	18.56	0.9828

q_{max} *(mg* g^{-1}*),* K_D *(*mol^2 KJ^{-2}*),* E_D *(KJ* mol^{-1}*)*

Table 4. Temkin isotherm parameters for the adsorption of cadmium and lead ions onto adsorbents

Adsorbents	Cadmium			Lead		
	b_T	A_T	R^2	b_T	A_T	R^2
Ch@F	337.688	8.7597	0.9761	47.685	9.6901	0.9935
Ch@EDTA@F	310.146	99.484	0.9889	30.991	9.6545	0.9946
Ch@EDTA@Am.@F	28.834	0.0613	0.9951	14.220	0.0315	0.9972

b_T (J mol^{-1}) , A_T (L mg^{-1})

3.8. Adsorption kinetics

Two kinetic models were tested to interpret the mechanism of adsorption of cadmium and lead ions onto Ch@F, Ch@EDTA@F, and Ch@EDTA@Am@F. The first model was pseudo-first-order; the mathematical expression of this model is given by Equation 10.

$$\ln(q_e - q_t) = lnq_1 - k_1 t \qquad \text{(Eq.10)}$$

Where q_t and q_1 (in mg g^{-1}) are the amounts of dye adsorbed at time t, and equilibrium, respectively, and k_1 (in min^{-1}) is the pseudo-first-order rate constant for adsorption. Figures 15 and 16 (A, B, C) represent the pseudo-first-order kinetics of cadmium and lead ions onto prepared adsorbents, respectively, by plotting ln(qe-qt) on the Y-axis against t; the slope and intercept of the plot give K_1 and q_1. Table 5 displays the values of calculated adsorption rate constants k1, maximum adsorption capacity q1, and correlation coefficient R^2. A second kinetic model is the Pseudo-second order, which can be expressed in linear form as Equation 11 [45,46].

$$\frac{t}{q_t} = \frac{1}{k_2 q_2^2} + \frac{t}{q_2} \qquad \text{(Eq.11)}$$

Where q_2 is the maximum adsorption capacity for the pseudo-second-order and k_2 is the equilibrium rate constant for pseudo-second-order adsorption. Figures 17 and 18 (A, B, C) represent the pseudo-second-order kinetics of cadmium and lead ions onto the prepared adsorbents, respectively. By plotting t/qt on the Y-axis against t, the slope and intercept of the plot provide k_2 and q_2. Table 6 displays the values of calculated adsorption rate constants k_2, maximum adsorption capacity q_2, and correlation coefficient R^2.

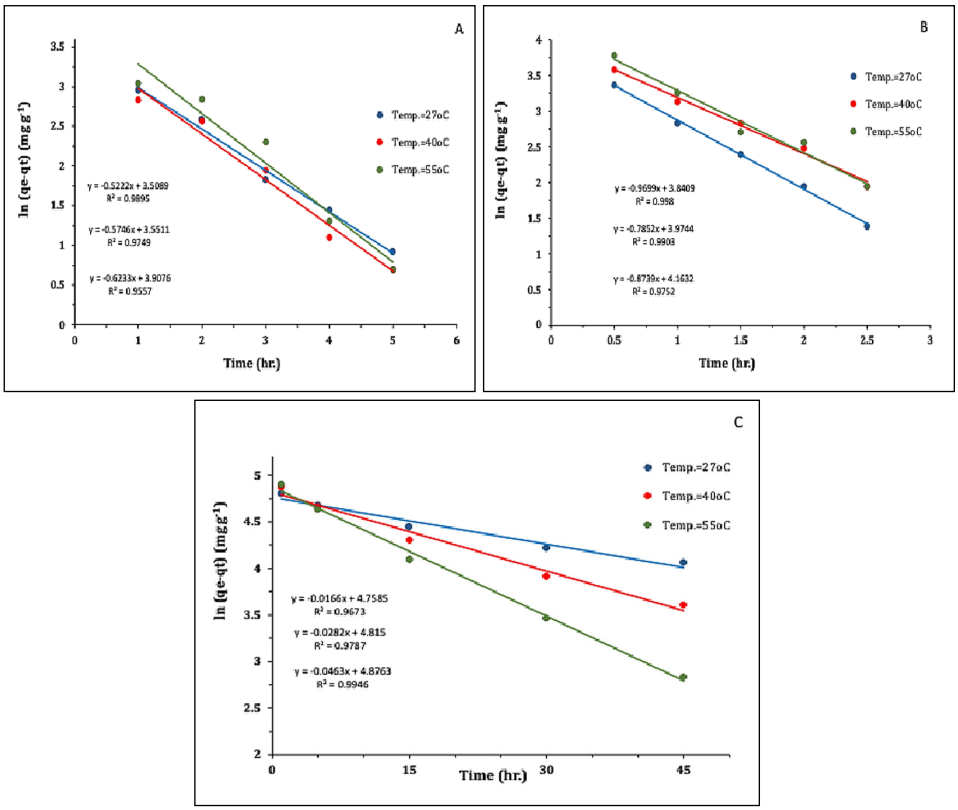

Fig. 15. Pseudo-First-Order for Cadmium ion onto (A): Ch@F (B): Ch@EDTA@F (C) Ch@EDTA@Am@F at 27°C, 40°C and 55°C

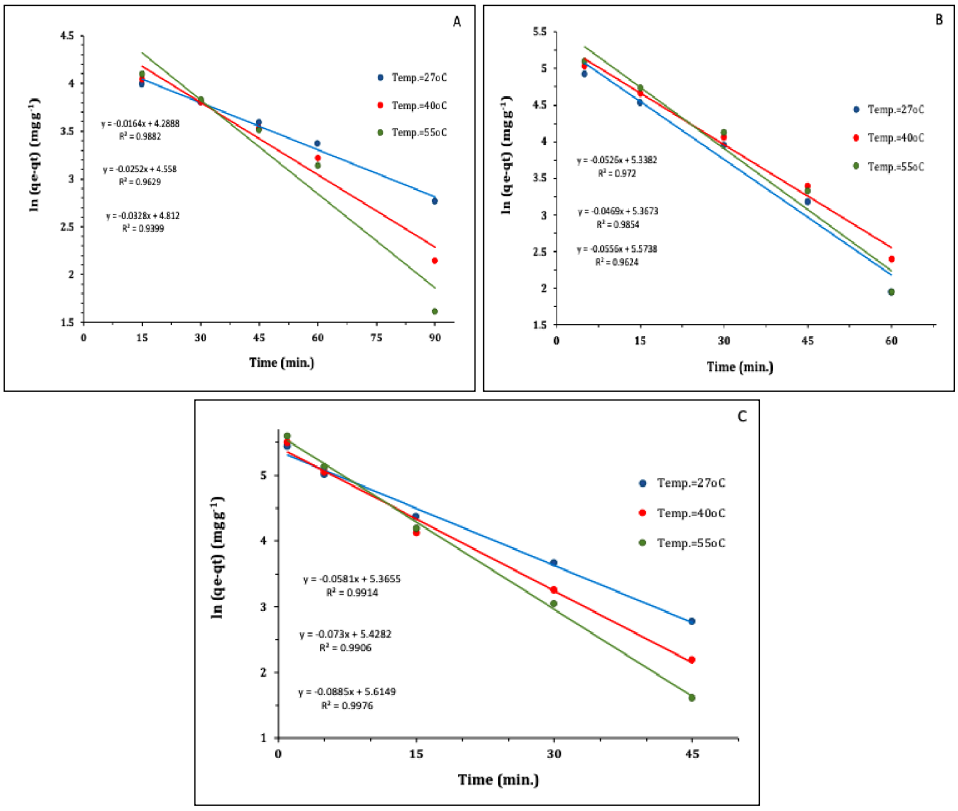

Fig. 16. Pseudo-First-Order for Lead ion onto (A): Ch@F (B): Ch@EDTA@F C) Ch@EDTA@Am@F at 27 °C, 40 °C, and 55 °C.

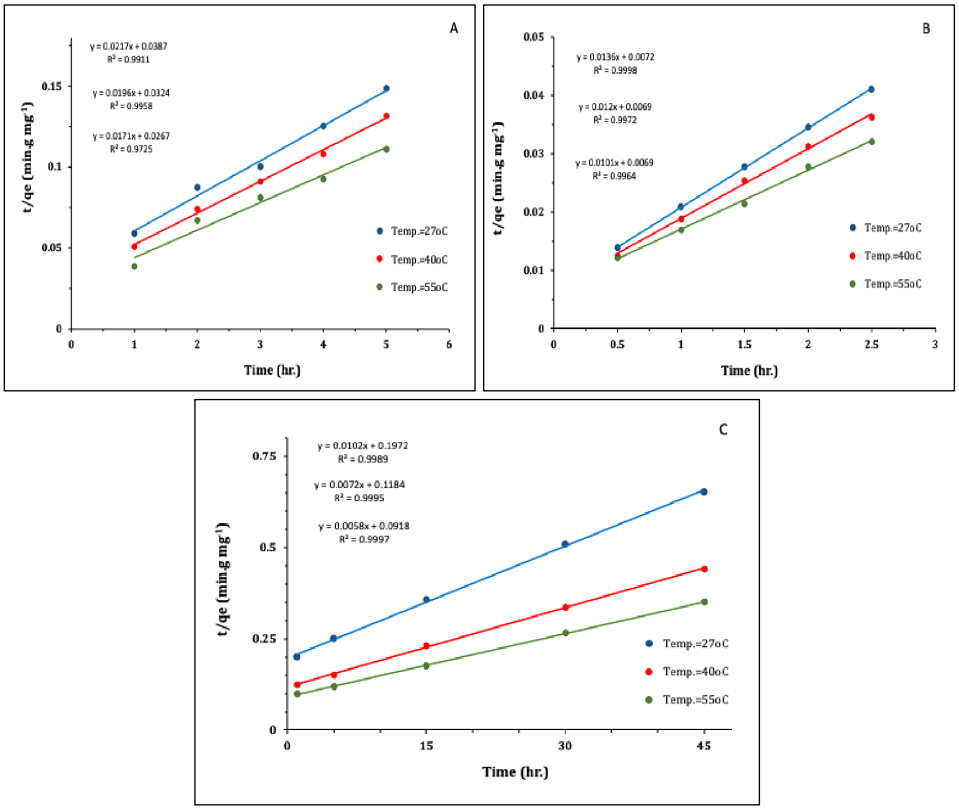

Fig. 17. Pseudo-Second-Order for Cadmium ion onto (A): Ch@F (B): Ch@EDTA@F (C) Ch@EDTA@Am.@F at 27°C, 40°C and 55°C.

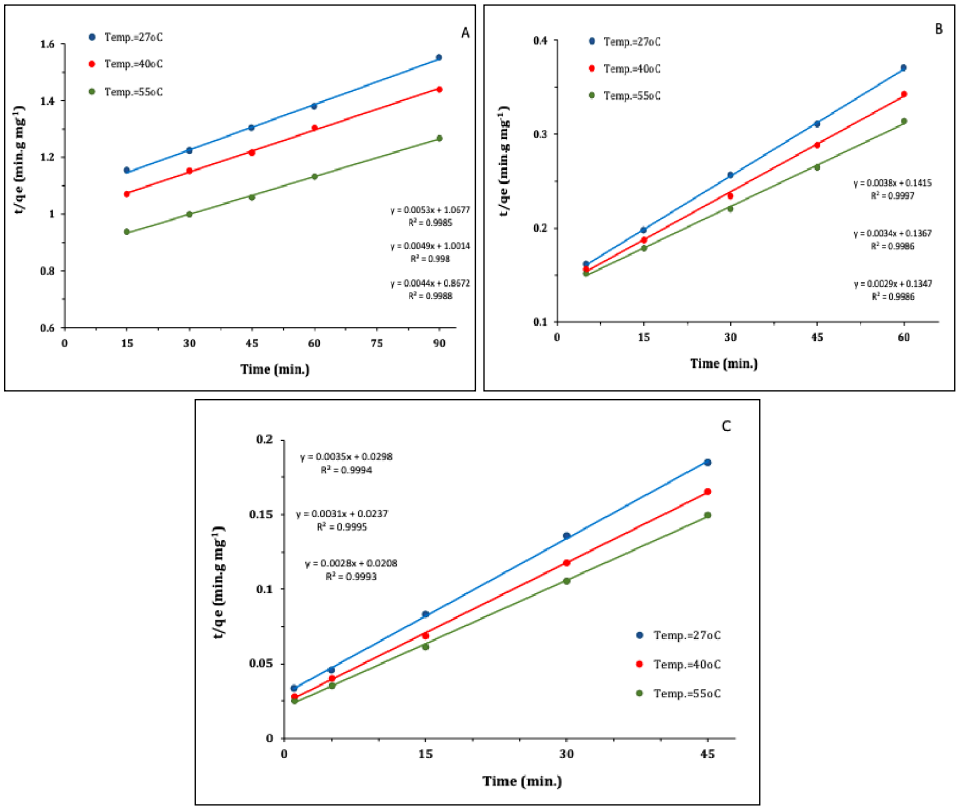

Fig.18.Pseudo-Second-Order for Lead ion onto (A): Ch@F (B): Ch@EDTA@F C) Ch@EDTA@Am.@F at 27°C, 40°C and 55°C.

Table 5. Pseudo-first-order parameters for the absorption of Cd and Pb in different temperatures

Adsorbents		Cadmium			Lead		
	T(°C)	k_1	q_1	R^2	k_1	q_1	R^2
Ch@F	27	0.5222	33.412	0.9895	0.0164	72.879	0.9882
	40	0.5746	34.852	0.9749	0.0252	95.393	0.9629
	55	0.6233	49.779	0.9557	0.0328	122.977	0.9399
Ch@EDTA@F	27	0.9699	46.567	0.998	0.0526	208.138	0.972
	40	0.7852	53.218	0.9903	0.0469	214.284	0.9854
	55	0.8205	64.277	0.9728	0.0556	263.433	0.9624
Ch@EDTA@Am.@F	27	0.0166	116.57	0.9661	0.0581	213.898	0.9914
	40	0.0282	123.35	0.9765	0.073	227.739	0.9906
	55	0.0463	131.15	0.9826	0.0885	274.486	0.9880

k1 (min^{-1}), q (mg g^{-1})

Table 6. Pseudo-second-order parameters for the absorption of Cd and Pb at different temperatures

Adsorbents		Cadmium			Lead		
	T (°C)	k_2	q_2	R^2	k_2	q_2	R^2
Ch@F	27	0.01217	46.083	0.9911	2.6E-05	188.679	0.9985
	40	0.01186	51.020	0.9887	2.4E-05	204.082	0.998
	55	0.01095	58.480	0.9725	2.2E-05	227.273	0.9988
Ch@EDTA@F	27	0.02569	73.529	0.9998	1.0E-04	263.158	0.9997
	40	0.02087	83.333	0.9972	8.4E-05	294.118	0.9986
	55	0.01478	99.010	0.9964	6.2E-05	344.828	0.9986
Ch@EDTA@ Am.@F	27	0.00053	98.039	0.9988	4.1E-04	285.714	0.9994
	40	0.00046	135.135	0.9948	4.5E-04	322.581	0.9995
	55	0.0004	172.414	0.9997	0.000377	357.143	0.9993

3.9. Adsorption thermodynamics

Thermodynamic parameters can be determined from the thermodynamic equilibrium constant, K_L (or the thermodynamic distribution coefficient) [47], whereas K_L *is* calculated in Equation 12.

$$K_L = \frac{C_a}{C_e} \qquad \text{(Eq. 12)}$$

Where C_a and C_e are the equilibrium concentrations of metal ions (in mg g^{-1}) and in the solution (mg L^{-1}), respectively. The standard enthalpy changes $\Delta H°$ (in kJ mol^{-1}) and standard entropy change) $\Delta S°$ (in J $mol^{-1}K^{-1}$) were calculated using the following Equation 13 [48].

$$\ln k = \frac{\Delta S^o}{R} - \frac{\Delta H^o}{RT} \qquad \text{(Eq. 13)}$$

Where R is the universal gas constant (8.314 J $mol^{-1}K^{-1}$), and T is the absolute temperature, plotting (lnKL) vs. (1/T) allows for the calculation of ΔH° from the slope and ΔS° from the intercept (Figures 19 A and 19B). The standard Gibbs free energy ΔG° (in kJ mol^{-1}) could be calculated at different temperatures from the following Equation 14 [49].

$$\Delta G^o = \Delta H^o - T\Delta S^o \qquad \text{(Eq. 14)}$$

Activation energy *Ea* (kJ mol^{-1}), which is defined as the minimum amount of energy required for the adsorption process to proceed [50], was calculated from the Arrhenius Equation 15 [51].

$$ln\ K = ln\ A - \frac{E_a}{RT} \qquad \text{(Eq. 15)}$$

Where K (g mg^{-1} min^{-1}) is the rate constant of the pseudo-second order adsorption systems, A is the Arrhenius factor, when (lnK) is plotted against (1/T), a slope equal to -*Ea*/R as shown in Figures 20 A and 20 B. The values of ΔH°, ΔS°, ΔG°, and Ea for the adsorption of metal ions onto adsorbents Ch@F, Ch@EDTA@F, and Ch@EDTA@Am@F are given in Table 7.

The calculated thermodynamic parameters show positive values of enthalpy (ΔH°) for all adsorbents, indicating the adsorption processes were endothermic. Also, the positive value of entropy (Δ*S*°) suggests an increase in the randomness at the (adsorbents/solution) interface and affinity of the mentioned adsorbents towards metal ions [52]. The obtained values of Gibbs free energy changes, ΔG°, at different temperatures were negative values for all adsorption systems, indicating the behavior of adsorption processes is spontaneous and feasible [53]. Low activation energy *Ea* values (<40 kJ.mol^{-1}) are characteristics of the physisorption mechanism. Whereas higher activation energies > 40 KJ mol^{-1} suggest chemisorption [54]. Therefore, these results indicate that the adsorption processes of metal ions onto Ch@F, Ch@EDTA@F, and Ch@EDTA@Am@F were physical. Also, some adsorbents, such as TSIL immobilized on multiwall carbon nanotubes, were used for the adsorption processes of metals [55].

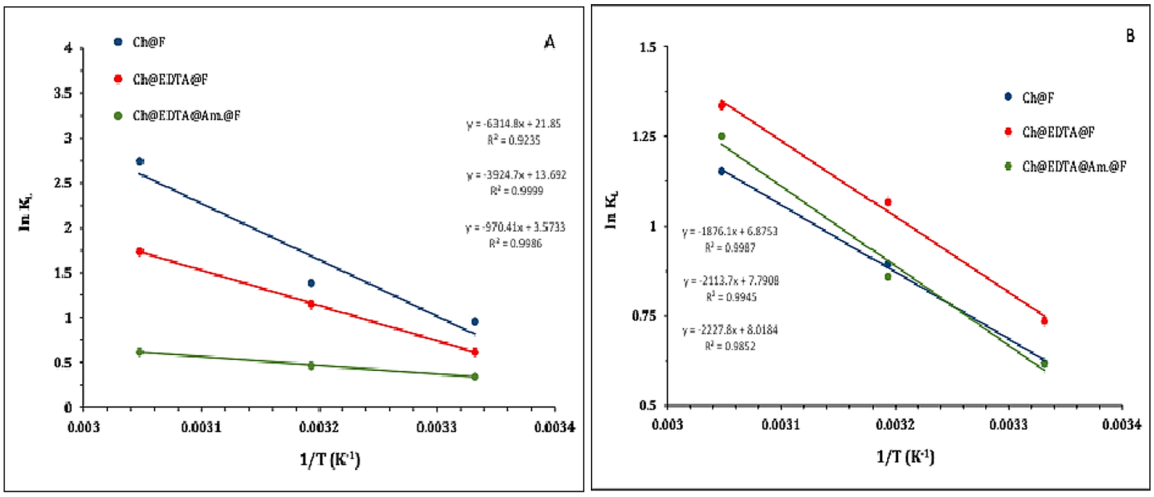

Fig. 19. Thermodynamic parameter determination for (A): Cadmium (B): Lead ion solution at 27°C

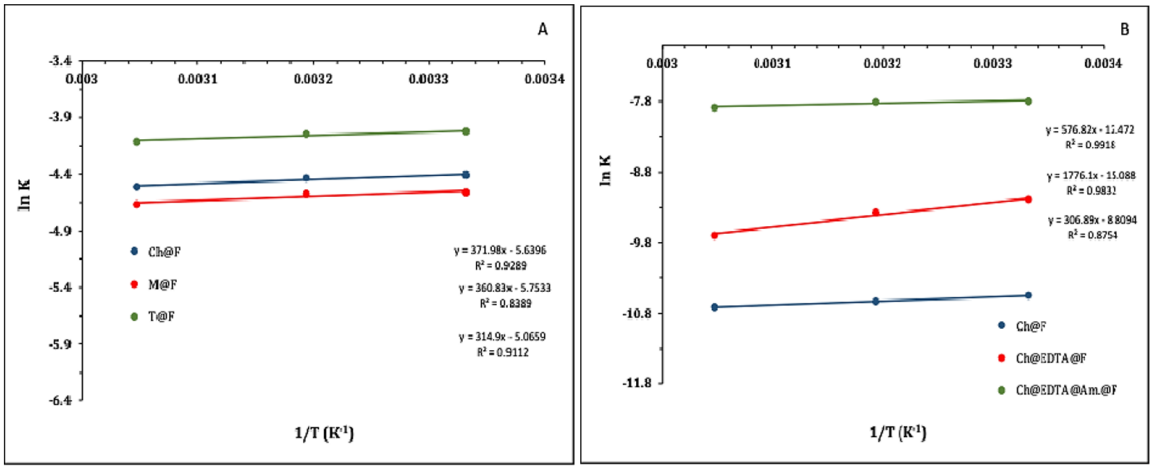

Fig. 20. Plot of lnK vs. 1/K of Arrhenius equation for (A): Cadmium (B): Lead ion solution at 27 °C

Table 7. Thermodynamic parameters for the adsorption of Cd and Pb onto adsorbents

Adsorbents	Cadmium					Lead			
	T(°K)	ΔH°	ΔS°	-ΔG°	Ea	ΔH°	ΔS°	-ΔG°	Ea
Ch@F	300.15	52.501	0.1816	-2.024	-3.09	15.5979	0.05716	-1.5591	-4.7957
	313.15			-4.386				-2.3022	
	328.15			-7.111				-3.1596	
Ch@EDTA@F	300.15	30.136	0.1138	-4.032	-16.19	17.573	0.0647	-1.8682	-14.766
	313.15			-5.512				-2.7103	
	328.15			-7.219				-3.6819	
Ch@EDTA@Am@F	300.15	12.121	0.04518	-1.439	-10.683	18.5219	8.0184	-1.4876	-2.5515
	313.15			-2.027				-2.3542	
	328.15			-2.705				-3.3542	

4. Conclusions

In this study, three magnetic nanocomposites Ch@F, Ch@EDTA@F, and Ch@EDTA@Am@F were examined to assess their ability to remove Cd^{2+} and Pb^{2+}. The maximum adsorption of metal ions onto the prepared adsorbents occurred at 27 °C and pH 8.0 for cadmium and 5.0 for lead. The adsorption capacity for metal ions increased with higher initial concentrations. The kinetic modeling of Cd^{2+} and Pb^{2+} adsorption onto the prepared adsorbents closely followed the pseudo-second-order rate model, with correlation coefficients above 0.99. Adsorption behavior is described by monolayer Langmuir-type isotherms for Ch@F, Ch@EDTA@F, and Ch@EDTA@Am@F. The calculated thermodynamic parameters show positive values of enthalpy (ΔH°) for all adsorbents, indicating the adsorption processes were endothermic. Also, the positive value of entropy (Δ*S*°) suggests an increase in the randomness at the (adsorbents/solution) interface and affinity of the mentioned adsorbents towards metal ions. The negative values ΔG° at different temperatures indicate that the behavior of adsorption processes is spontaneous and feasible. Low activation energy *Ea* values are characteristics of the physisorption mechanism and diffusion-controlled process. Pb and Cd ions were determined in solutions by flame atomic absorption spectrometry (F-AAS), with LODs of 3.3 µg L^{-1} and 0.58 µg L^{-1}, respectively. Additionally, the linear ranges of cadmium and lead were obtained at 2–300 µg L^{-1} and 10–1500 µg L^{-1}, respectively.

5. References

[1] J. Briffa, E. Sinagra, R. Blundell, Heavy metal pollution in the environment and their toxicological effects on humans, Heliyon, 6 (2020) e04691. https://doi.org/10.1016/j.heliyon.2020.e04691

[2] H. Mehtab, F. Muhammad, J. Asma, A. Sidra, A. Nayab, Z. Sharon, H. Jaweria, A review article of water pollution and human health, Environ. Risk Assess Remediate, 1 (2017) 16-19. https://doi.org/10.4066/2529-8046.100020

[3] S. Mahipal, K. Mayuri, N. Manisha, K. Rajeev, A. Prashant, A Review of heavy metals contamination in water and their hazardous effect on human health, Int. J. Current Microbiol. Appl. Sci., 5 (2016) 759-766.. http://doi.org/10.20546/ijcmas.2016.510.082

[4] N. Esmaeili, J. Rakhtshah, E. Kolvari, A. Rashidi, H. Shirkhanloo, Rapid speciation of lead in human blood and urine samples based on MWCNTs@DMP by dispersive ionic liquid-suspension-micro-solid phase extraction, Biol. Trace Elem. Res., 199 (2021) 2496–2507. https://doi.org/10.1007/s12011-020-02382-7

[5] M. Arjomandi, A review: analytical methods for heavy metals determination in environment and human samples, Anal. Methods Environ.

Chem. J., 2 (2019) 97-126. https://doi.org/10.24200/amecj.v2.i03.73

[6] M. K. Abbasabadi, F. Hosseini, Nanographene oxide modified phenyl methanethiol nanomagnetic composite for rapid separation of aluminum in wastewaters, foods, and vegetable samples by microwave dispersive, Food Chem., 347 (2021) 129042. https://doi.org/10.1016/j.foodchem.2021.129042

[7] S. D. Ahranjani, A lead analysis based on amine-functionalized bimodal mesoporous silica nanoparticles in human biological samples by ultrasound assisted-ionic liquid trap-micro solid phase extraction, J. Pharm. Biomed. Anal., 157 (2018) 1-9. https://doi.org/10.1016/j.jpba.2018.05.004

[8] M. K. Abbasabadi, Speciation of cadmium in human blood samples based on Fe_3O_4-supported naphthalene-1-thiol-functionalized graphene oxide nanocomposite by ultrasound-assisted dispersive magnetic micro solid phase extraction, J. Pharm. Biomed. Anal., 189 (2020) 113455. https://doi.org/10.1016/j.jpba.2020.113455

[9] F. Zarandi, An immobilization of 2-(Aminomethyl) thiazole on MWCNTs used for rapid extraction of manganese ions in hepatic patients, J. Pharm. Biomed. Anal., 240 (2024) 115941. https://doi.org/10.1016/j.jpba.2023.115941

[10] F. Zarandi, P. Paydar, A novel method based on functionalized bimodal mesoporous silica nanoparticles for efficient removal of lead aerosols pollution from air by solid-liquid gas-phase extraction, J. Environ. Health Sci. Eng., 18 (2020) 177–188. https://doi.org/10.1007/s40201-020-00450-7

[11] K. Sul, S. Jagadeesh, M. Sri, J. Seong, C. Woo, A. Ibrahim, K. Hyun-Kyung, Nano-Fe_3O_4/Carbon nanotubes composites by one-Pot microwave solvothermal method for supercapacitor applications, Energies, 14 (2021) 2908. http://doi.org/10.3390/en14102908

[12] L. Li, C. Luo, X. Li, H. Duan, X. Wang, Preparation of magnetic ionic liquid/chitosan/graphene oxide composite and application for water treatment, Int. J. Biol. Macromol., 66 (2014) 172-178. http://doi.org/10.1016/j.ijbiomac.2014.02.031

[13] D. Depan, B. Girase, J. Shah, R. Misra, Structure–process–property relationship of the polar graphene oxide-mediated cellular response and stimulated growth of osteoblasts on hybrid chitosan network structure nanocomposite scaffolds, Acta Biomater., 7 (2011) 3432-3445. http://doi.org/ 10.1016/j.actbio.2011.05.019

[14] M. Alaa, Preparation of graphene oxide-grafted polymers and the analytical study of their interaction with Congo Red and Bismarck brown dyes, Ph.D. Thesis, University of Basra, Iraq, 2020. https://en.hs.uobasrah.edu.iq/Theses

[15] Q. Nada, Synthesis and characterization of some new 1,3 thiazines and their complexes and evaluation of their adsorption capacity for water remediation, MSc. Thesis, University of Basra, Iraq, 2019. https://en.hs.uobasrah.edu.iq/Theses

[16] S. Huda. Adsorption study for removing some hazardous dyes by using hydrogels based on acrylamide, Ph.D. Thesis, University of Basra, Iraq, 2021. https://en.hs.uobasrah.edu.iq/Theses

[17] R. Yong, A. Hayder, H. Fengbo, P. Hong, H. Kaixun, Magnetic EDTA-modified chitosan/SiO_2/Fe_3O_4 adsorbent: Preparation, characterization, and application in heavy metal adsorption, Chem. Eng. J., 226 (2013) 300–311. http://doi.org/10.1016/j.cej.2013.04.059

[18] D. Pavia, G. Lampman, G. Kriz, J. Vyvyan, Introduction to spectroscopy, Cengage Learning, book, Thomson Learning, Third Edition, ISBN: 0-03-031961-7, 2008. http://dl.iranchembook.ir/ebook/organic-chemistry-2753.pdf

[19] M. Ghorbani, A. Shams, O. Seyedin, N. Lahoori, Magnetic ethylene diaminefunctionalized graphene oxide as novel sorbent for removal of lead and cadmium ions from wastewater samples, Environ. Sci. Pollut. Res. 25 (2018) 5655-5667. http://doi.org/10.1007/s11356-017-0929-7

[20] A. Monshi, M. Foroughi, M. Monshi, Modified Scherrer equation to estimate more accurately nanocrystallite size using XRD, World J. Nano Sci. Eng., 2 (2012) 154–160. http://doi.org/10.4236/wjnse.2012.23020

[21] M. Ahamed, H. A. Alhadlaq, M. Khan, P. Karuppiah, N. Al-Dhabi, Synthesis, Characterization, and antimicrobial activity of copper oxide nanoparticles, J. Nanomater., 2014 (2014) 1–4. http://doi.org/10.1155/2014/637858

[22] Y. Ahmed, Preparation and characterization of some Ferrite spinal magnetic nanocomposites and their use as adsorbent surfaces to treat elemental and oil pollution from their aqueous solutions, University of Basrah, Thesis, 2021. https://en.ceps.uobasrah.edu.iq/news/11152

[23] O. Al-Gohary, In vitro adsorption of mebeverine hydrochloride onto kaolin and its relationship to pharmacological effects of the drug in vivo, Pharm. Acta Helv., 72 (1997) 11-22. http://doi.org/10.1016/s0031-6865(96)00042-8

[24] L. Cruz-Lopes, M. Macena, B. Esteves, R. Guine, Optimization and thermodynamic studies of lead (II) and cadmium (II) ions removal from water using Musa acuminate pseudo-stem biochar, Open Agric., 6 (2021) 115-123. http://doi.org/10.4236/gsc.2023.134014

[25] A. Rashidi, A. Vahid, Arsenic speciation based on amine-functionalized bimodal mesoporous silica nanoparticles by ultrasound assisted-dispersive solid-liquid multiple phase microextraction, Microchem. J., 130 (2017) 137-146. https://doi.org/10.1016/j.microc.2016.08.013

[26] C. Shih, J. Park, D. Sholl, M. Realff, T. Yajima, Y. Kawajiri, Hierarchical Bayesian estimation for adsorption isotherm parameter determination, Chem. Eng. Sci., 214 (2020) 115435. http://doi.org/10.1016/j.ces.2019.115435

[27] Y. Kuang, X. Zhang, S. Zhou, Adsorption of methylene blue in water onto activated carbon by surfactant modification, Water (Switzerland), 12 (2020) 1–19. http://doi.org/10.3390/w12020587

[28] K. Foo, B. Hameed, Insights into the modeling of adsorption isotherm systems, Chem. Eng. J., 156 (2010) 2–10. https://doi.org/10.1016/j.cej.2009.09.013

[29] A. H. Sulaymon, T. Mohammed, J. Al-Najar, Equilibrium and kinetics studies of adsorption of heavy metals onto activated carbon, Can. J. Chem. Eng. Technol., 3 (2012) 86–92. https://onlinelibrary.wiley.com/loi/1939019x

[30] A.A. Ansari, S.S. Gill, R. Gill, G. R. Lanza, L. Newman. Phytoremediation, Management of Environmental Contaminants, Springer, 2016. https://doi.org/10.1007/978-3-319-10395-2

[31] M. Temkin, V. Pyzhev, Application of Temkin adsorption isotherm, Acta Physiochim., 12 (1940) 217-222. http://doi.org/10.4236/ajcm.2012.23030

[32] Y. Meshram, J. Gunjate, R. Khope, Studies on adsorption characteristics of manganese onto coal based chemically modified activated carbon, Mater. Today: Proc., 29 (2020) 1185-1191. http://doi.org/10.1016/j.matpr.2020.05.428

[33] M. Dubinin, Physical adsorption of gases and vapors in micropores, Progress in surface and membrane science, Elsevier, 9 (1975) 1-70. http://doi.org/10.1016/B978-0-12-571809-7.50006-1

[34] S. Rengaraj, J. Yeon, Y. Kim, Y. Jung, Y. Ha, W. Kim, Adsorption characteristics of Cu(II) onto ion exchange resins 252H and 1500H: Kinetics, isotherms and error analysis, J. Hazard. Mater., 143 (2007) 469–477. http://doi.org/10.1016/j.jhazmat.2006.09.064

[35] R. Gautam, A. Mudhoo, G. Lofrano, M. Chattopadhyaya, Biomass-derived biosorbents for metal ions sequestration: Adsorbent modification and activation methods and adsorbent regeneration, J. Environ. Chem. Eng., 2 (2013) 239–259. http://doi.org/10.1016/j.jece.2013.12.019

[36] C. Hussain, Nanomaterials in chromatography: current trends in chromatographic research technology and techniques, Elsevier, 2018. https://doi.org/10.1016/C2016-0-04157-8

[37] N. Esmaeili, J. Rakhtshah, Ultrasound assisted-dispersive-modification solid-phase extraction using task-specific ionic liquid immobilized on multiwall carbon nanotubes for speciation

and determination mercury in water samples, Microchem. J., 154 (2020) 104632. https://doi.org/10.1016/j.microc.2020.104632

[38] P. Luo, B. Zhang, Y. Zhao, J. Wang, H. Zhang, J. Liu, Removal of methylene blue from aqueous solutions by adsorption onto chemically activated halloysite nanotubes, Korean J. Chem. Eng., 28 (2011) 800–807. http://doi.org/10.1007/s11814-010-0426-x

[39] R. García, R. Medina, M. Lozano, I. Pérez, M. Valero, A. Maubert, Adsorption of azo-dye Orange II from aqueous solutions using a metal-organic framework material: Iron-benzenetricarboxylate, Materials, 7 (2014) 8037–8057. http://doi.org/10.3390/ma7128037

[40] A. Muhammad, Adsorption of methylene blue onto modified agricultural waste, Mor. J. Chem., 8 (2020) 412-427. http://doi.org/10.48317/IMIST.PRSM/morjchem-v8i2.16692

[41] X. Lv, S. Li, Graphene oxide–crospolyvinyl pyrrolidone hybrid microspheres for the efficient adsorption of 2, 4, 6-Trichlorophenol, ACS Omega., 5 (2020) 18862–18871. http://doi.org/10.1021/acsomega.0c02028

[42] F. Togue, Modeling adsorption mechanism of paraquat onto Ayous (Triplochiton scleroxylon) wood sawdust, Appl. Water Sci., 9 (2019) 1. https://doi.org/10.1007/s13201-018-0879-3

[43] H. Joga, P. King, Y. Prasanna, Application of response surface methodology for optimization of cadmium adsorption in an aqueous solution by activated carbon prepared from Bauhinia Purpurea leaves, RASAYAN J. Chem., 11(2018) 1577–1586. https://doi.org/10.31788/RJC.2018.1144024

[44] K. Shahjalal, T. Yusaku, C. Ganesh, R. Md. K. Takahiro, Development of synthetic zeolites from bio-slag for cesium adsorption: Kinetic, isotherm and thermodynamic studies, J. Water Process Eng., 33 (2020) 101055. https://doi.org/10.1016/j.jwpe.2019.101055

[45] S. Davari, F. Hosseini, Dispersive solid-phase microextraction based on amine functionalized bimodal mesoporous silica nanoparticles for separation and determination of calcium ions in chronic kidney disease, Anal. Methods Environ. Chem. J., 1 (2018) 57-66. https://doi.org/10.24200/amecj.v1.i01.37

[46] Y. Ho, G. McKay, Pseudo-second order model for sorption processes, Process Biochem., 34 (1999) 451–465. https://doi.org/10.1016/S0032-9592(98)00112-5

[47] F. Golbabaei, Z. Sadeghi, A. Vahid, A. Rashidi, On-line micro column preconcentration system based on amino bimodal mesoporous silica nanoparticles as a novel adsorbent for removal and speciation of chromium (III, VI) in environmental samples, J. Environ. Health Sc. Eng., 13 (2015) 1-12. https://doi.org/10.1186/s40201-015-0205-z

[48] Y. Özdemir, M. Doğan, M. Alkan, Adsorption of cationic dyes from aqueous solutions by sepiolite, Micropor. Mesopor. Mater., 96 (2006) 419-427. https://doi.org/10.1016/j.micromeso.2006.07.026

[49] H. Tran, S. You, H. Chao, Thermodynamic parameters of cadmium adsorption onto orange peel calculated from various methods: a comparison study, J. Environ. Chem. Eng., 4 (2016) 2671-2682. http://doi.org/10.1016/j.jece.2016.05.009

[50] O. Akinbulumo, O. Odejobi, E. Odekanle, Thermodynamics and adsorption study of the corrosion inhibition of mild steel by Euphorbia heterophylla L. extract in 1.5 M HCl, Results Mater., 5 (2020) 100074. http://doi.org/10.1016/j.rinma.2020.100074

[51] M. Ahmad, N. Puad, O. Bello, Kinetic, equilibrium and thermodynamic studies of synthetic dye removal using pomegranate peel activated carbon prepared by microwave-induced KOH activation, Water Resour. Ind., 6 (2014) 18-35. http://doi.org/10.1016/j.wri.2014.06.002

[52] Y. Önal, C. Akmil-Başar, D. Eren, C. Sarıcı-Özdemir, T. Depci, Adsorption kinetics of malachite green onto activated carbon prepared from Tunçbilek lignite, J. Hazard. Mater., 128 (2006) 150-157. http://doi.org/10.1016/j.jhazmat.2005.07.055

[53] D. Lin, F. Wu, Y. Hu, T. Zhang, C. Liu, Q. Hu, Y. THu, Z. Xue, H. Han, T. Ko, Adsorption of dye by waste black tea powder: parameters, kinetic, equilibrium, and thermodynamic studies, J. Chem., 2020 (2020) 5431046. http://doi.org/10.1155/2020/5431046

[54] A. Swelam, M. Awad, Y. Gedamy, A. Tawfik, Fe_3O_4 nanoparticles: Synthesis, characterization and application in removal of iron from aqueous solution and groundwater, Egypt. J. Chem., 62 (2019) 1189–1209. http://doi.org/10.21608/EJCHEM.2019.5527.1488

[55] N. Esmaeili, J. Rakhtshah, Ultrasound assisted-dispersive-modification solid-phase extraction using task-specific ionic liquid immobilized on multiwall carbon nanotubes for speciation and determination mercury in water samples, Microchem. J., 154 (2020) 104632. https://doi.org/10.1016/j.microc.2020.104632